

# The Optically Unbiased GRB Host (TOUGH) survey. IV. Lyman- $\alpha$ emitters\*

Bo Milvang-Jensen<sup>1</sup>, Johan P. U. Fynbo<sup>1</sup>, Daniele Malesani<sup>1</sup>, Jens Hjorth<sup>1</sup>, Páll Jakobsson<sup>2</sup>, and Palle Møller<sup>3</sup>  
milvang@dark-cosmology.dk

## ABSTRACT

We report the results of a spectroscopic search for Lyman- $\alpha$  ( $\text{Ly}\alpha$ ) emission from gamma-ray burst (GRB) host galaxies. Based on a well-defined parent sample (the TOUGH sample) of 69 X-ray selected *Swift* GRBs, we have targeted the hosts of a subsample of 20 GRBs known from afterglow spectroscopy to be in the redshift range  $z = 1.8\text{--}4.5$ . We have obtained spectroscopy using the FORS1 instrument at the ESO Very Large Telescope to search for the presence of  $\text{Ly}\alpha$  emission from the host galaxies. We detect  $\text{Ly}\alpha$  emission from 7 out of the 20 hosts, with the typical limiting  $3\sigma$  line flux being  $8 \times 10^{-18} \text{ erg cm}^{-2} \text{ s}^{-1}$ , corresponding to a  $\text{Ly}\alpha$  luminosity of  $6 \times 10^{41} \text{ erg s}^{-1}$  at  $z = 3$ . The  $\text{Ly}\alpha$  luminosities for the 7 hosts in which we detect  $\text{Ly}\alpha$  emission are in the range  $(0.6\text{--}2.3) \times 10^{42} \text{ erg s}^{-1}$ , corresponding to star-formation rates of  $0.6\text{--}2.1 M_{\odot} \text{ yr}^{-1}$  (not corrected for extinction). The rest-frame  $\text{Ly}\alpha$  equivalent widths (EWs) for the 7 hosts are in the range  $9\text{--}40 \text{ \AA}$ . For 6 of the 13 hosts for which  $\text{Ly}\alpha$  is not detected we place fairly strong  $3\sigma$  upper limits on the EW ( $< 20 \text{ \AA}$ ), while for others the EW is either unconstrained or has a less constraining upper limit. We find that the distribution of  $\text{Ly}\alpha$  EWs is inconsistent with being drawn from the  $\text{Ly}\alpha$  EW distribution of bright Lyman break galaxies (LBGs) at the 98.3% level, in the sense that the TOUGH hosts on average have *larger* EWs than bright LBGs. We can exclude an early indication, based on a smaller, heterogeneous sample of pre-*Swift* GRB hosts, that all GRB hosts are  $\text{Ly}\alpha$  emitters. We find that the TOUGH hosts on average have *lower* EWs than the pre-*Swift* GRB hosts, but the two samples are only inconsistent at the 92% level. The velocity centroid of the  $\text{Ly}\alpha$  line (where detected) is redshifted by  $200\text{--}700 \text{ km s}^{-1}$  with respect to the systemic velocity (taken to be the afterglow redshift), similar to what is seen for LBGs, possibly indicating star-formation driven outflows from the host galaxies. There seems to be a trend between the  $\text{Ly}\alpha$  EW and the optical to X-ray spectral index of the afterglow ( $\beta_{\text{OX}}$ ), hinting that dust plays a role in the observed strength and even presence of  $\text{Ly}\alpha$  emission.

*Subject headings:* dust, extinction — galaxies: fundamental parameters — galaxies: high-redshift — galaxies: star formation — gamma-ray burst: general — surveys

---

\*Based on observations collected at the European Southern Observatory, Chile, as part of program 177.A-0591.

<sup>1</sup>Dark Cosmology Centre, Niels Bohr Institute, University of Copenhagen, Juliane Maries Vej 30, 2100 Copenhagen Ø, Denmark

<sup>2</sup>Centre for Astrophysics and Cosmology, Science Institute, University of Iceland, Dunhagi 5, 107 Reykjavík, Iceland

<sup>3</sup>European Southern Observatory, Karl-Schwarzschild-Strasse 2, 85748 Garching bei München, Germany

## 1. Introduction

Due to their potential brightness at wavelengths ranging from radio to gamma-rays, gamma-ray bursts (GRBs) and their afterglows can be used as powerful astrophysical probes. They are momentarily bright enough to be observed anywhere in the Universe, even if located in the most dusty environments or at the highest redshifts (e.g. Wijers et al. 1998), but later fade

away and allow a detailed study of their environment. It is now established that long-duration GRBs are associated with core collapse supernovae (e.g., Stanek et al. 2003; Hjorth et al. 2003; Woosley & Bloom 2006; Hjorth & Bloom 2012) and hence star-formation. GRBs thus can be used to probe the star-formation density over most of the cosmic history from the formation of the first stars to the present. The most spectacular example of this is GRB 090423 at  $z = 8.2$  (Tanvir et al. 2009; Salvaterra et al. 2009) representing a look-back time of more than 95% of the time since the Big Bang.

$\text{Ly}\alpha$ -emitting galaxies are in a state of active star-formation and most likely contain little or no dust, since  $\text{Ly}\alpha$  photons have a much higher probability than other UV photons of being absorbed by dust due to resonant scattering (Adams 1972; Charlot & Fall 1993; Valls-Gabaud 1993).  $\text{Ly}\alpha$  emission is hence sensitive to both the star-formation rate and the dust content of GRB host galaxies. In addition, geometrical effects and the kinematical state of the interstellar medium seem to be important for the escape of  $\text{Ly}\alpha$  photons (e.g., Giavalisco et al. 1996; Hayes et al. 2005; Verhamme et al. 2006; Laursen et al. 2009).

The first studies of  $\text{Ly}\alpha$  emission from (pre-*Swift*) GRB host galaxies indicated that  $\text{Ly}\alpha$  emission seemed to be ubiquitous, with 5 detections out of 5 possible (Fynbo et al. 2003)<sup>1</sup>. This would be intriguing as only about 25% of Lyman-break selected galaxies (LBGs) at similar redshifts have  $\text{Ly}\alpha$  emission with rest-frame equivalent width (EW) larger than 20 Å (Shapley et al. 2003); this is also the case at higher redshifts (Douglas et al. 2010, but see also Stark et al. 2011). Another 6 GRB host  $\text{Ly}\alpha$  emitters (all from *Swift* GRBs) have been reported in the literature since then<sup>2</sup> (excluding the hosts reported in this work<sup>3</sup>), but

<sup>1</sup>GRB 971214 (Kulkarni et al. 1998), GRB 000926 (Fynbo et al. 2002), GRB 011211 (Fynbo et al. 2003), GRB 021004 (Møller et al. 2002, and references therein), and GRB 030323 (Vreeswijk et al. 2004).

<sup>2</sup>GRB 060714 (Jakobsson et al. 2006b), GRB 060926 (Fynbo et al. 2009), GRB 061222A (Perley et al. 2009), GRB 070110 (Fynbo et al. 2009), GRB 071031 (Fynbo et al. 2009), and GRB 090205 (D’Avanzo et al. 2010).

<sup>3</sup>This work reports the detection of  $\text{Ly}\alpha$  emission from 7 host galaxies, of which one (GRB 070110) was already identified as a  $\text{Ly}\alpha$  emitter in the literature.

there still has not been a systematic examination of the frequency of  $\text{Ly}\alpha$  emitters among GRB host galaxies. This is the aim of the present work.

Given the effect of dust on  $\text{Ly}\alpha$  photons, possible explanations for an excess of  $\text{Ly}\alpha$  emitters among GRB host galaxies include (Fynbo et al. 2003): (i) a preference for GRB progenitors to be metal poor as expected in the collapsar model (Woosley & Heger 2006; Yoon & Langer 2005; see also Niino et al. 2009); (ii) an optical afterglow selection bias against dusty hosts; (iii) a higher fraction of  $\text{Ly}\alpha$  emitters at the faint end of the high-redshift luminosity function, where most GRB hosts are found; (iv) small-number statistics. Using a well selected and more complete *Swift* sample we shall here address these issues.

The paper is structured in the following way. The parent sample (TOUGH), the target selection, the spectroscopic observations and the data reduction are described in §2. The  $\text{Ly}\alpha$  detections and upper limits are presented in §3.1. The velocity offset of the  $\text{Ly}\alpha$  emission with respect to the systemic velocity as given by the afterglow redshift is discussed in §3.2. A comparison of the  $\text{Ly}\alpha$  fluxes from afterglow and host spectra is done in §3.3. In §4 we discuss the results, including how they relate to LBGs and to pre-*Swift* studies, and how the observed  $\text{Ly}\alpha$  emission is related to the afterglow broad-band spectral index  $\beta_{\text{OX}}$ , and we summarize our findings. Finally, the Appendix presents observations targeting the hosts of 3 GRBs that are not part of the complete, well defined TOUGH sample discussed in the main part of the paper.

We assume  $H_0 = 70 \text{ km s}^{-1} \text{ Mpc}^{-1}$ ,  $\Omega_m = 0.3$ ,  $\Omega_\Lambda = 0.7$ . This only affects the  $\text{Ly}\alpha$  luminosities and the derived star-formation rates. The reported magnitudes are on the Vega system, with the exception of Fig. 9.

The reduced data from this work will be available from ESO<sup>4</sup> and from the TOUGH website<sup>5</sup>.

<sup>4</sup><http://archive.eso.org/>

<sup>5</sup><http://www.dark-cosmology.dk/TOUGH>

## 2. Target selection, observations and data reduction

### 2.1. The TOUGH sample

This work is based on a parent sample named The Optically Unbiased GRB Host (TOUGH) sample. This sample of 69 *Swift* GRBs has several important features: (i) The selection criteria (see below) are designed to provide an optically unbiased (X-ray selected) sample of long-duration GRBs; (ii) The selection criteria are also designed to increase the prospects of prompt follow-up observations being successful; (iii) The sample has been the focus of an extensive prompt follow-up campaign by our group (e.g. Fynbo et al. 2009); (iv) The sample has been the focus of an extensive late-time follow-up campaign targeting the host galaxies, as reported in this series of papers (Hjorth et al. 2012; Malesani et al. 2012; Jakobsson et al. 2012; this paper; Krühler et al. 2012; Michałowski et al. 2012).

The sample selection criteria and their rationale are given in detail in Hjorth et al. (2012). They can be summarised as follows: (1) The burst should trigger the  $\gamma$ -ray imager BAT onboard *Swift*; (2) Only long-duration bursts are considered; (3) An X-ray afterglow should be detected and the *Swift* XRT X-ray position should be made available within 12 hours from the trigger; (4) Milky Way extinction  $A_V \leq 0.5$  mag; (5) Sun distance at the time of the GRB detection  $> 55^\circ$ ; (6) No nearby bright stars (would complicate host galaxy observations); (7) Only bursts in the period 2005 March 1 to 2007 August 10 are considered; (8) Declination in the range  $-70^\circ$  to  $+27^\circ$  (suitable for VLT observations); (9) The localization of the burst from the X-ray afterglow should be better than  $2.0''$  (90% error radius)<sup>6</sup>.

Furthermore, observations targeting the host as part of the TOUGH large program should be carried out at least 50 days after the GRB.

<sup>6</sup>This includes using the revised UVOT-enhanced *Swift*-XRT positions (Evans 2011; Evans & Osborne 2011), which has had the effect of increasing the sample size from 68 (e.g. Jakobsson et al. 2011) to 69, with the additional burst being GRB 060923B.

### 2.2. Target selection

The GRBs for the Ly $\alpha$  host galaxy spectroscopy studied here were selected from the TOUGH sample by applying the criterion that the (spectroscopic) redshift should be known and in the range 1.8 to 4.5. The lower limit comes from the atmospheric cut-off and the sensitivity curve of the used CCDs, while the upper limit comes from fringing in the CCDs used in some of the observing runs.

At the time of the target selection for the last run of the observing campaign for the Ly $\alpha$  spectroscopy (§2.3), the redshift status of the TOUGH sample was as follows: (a) 20 bursts met the  $z = 1.8$ –4.5 criterion, and these were the ones observed, as listed in Table 1. (b) 21 bursts had  $z$  outside the range 1.8–4.5. (c) 28 bursts did not have a secure, spectroscopic redshift determination. Note that group (b) included 5 redshifts obtained as part of the TOUGH redshift campaign (Jakobsson et al. 2012) which were available before the Ly $\alpha$  observing campaign ended.

For reference, the redshifts were subsequently revised for some bursts, and redshifts became available for other bursts. As of February 2012, the split of the TOUGH sample into the three groups based on redshift would be: (a') 27 hosts have  $z = 1.8$ –4.5, of which 20 hosts are those observed with FORS1 in the Ly $\alpha$  campaign and presented in this paper (Table 1), while 7 hosts do not have such FORS1 spectroscopy<sup>7</sup>. (b') 22 hosts have  $z$  outside 1.8–4.5. (c') 20 hosts do not have a (secure, spectroscopic) redshift.

The redshifts of two of the hosts included in our Ly $\alpha$  campaign warrant special mention. GRB 060604 was originally included because it had a tentative afterglow redshift of  $z = 2.68$  proposed by Castro-Tirado et al. (2006). A subsequent re-reduction and analysis of the same data by Fynbo et al. (2009) did not confirm that redshift. Instead, an upper limit of  $z \lesssim 3$  was derived, and a possible redshift of  $z = 2.124$  was suggested, based on a single absorption line interpreted as Al II. We recently obtained an X-shooter host spectrum (Krühler et al. 2012) that gives  $z \approx 2.1359$  from H $\beta$ , [O III] and H $\alpha$ . This

<sup>7</sup>These 7 additional bursts have redshifts from recent X-shooter host spectroscopy (Krühler et al. 2012, see also §4.2).

TABLE 1  
GRB SAMPLE AND LOG OF FORS1  $\text{Ly}\alpha$  HOST GALAXY OBSERVATIONS

Name	$z$	Ref.	$R_{\text{host}}$ (mag)	Grism+filter	CCD	$T_{\text{exp}}^{\text{total}}$ (hr)	Seeing (arcsec)	$A_V$ (mag)
GRB 050315	1.9500	(1)	24.4	600B	new	1.5	0.84	0.159
GRB 050401	2.8983	(2); (8)	26.1	600B	old	2.1	0.76	0.216
GRB 050730	3.96855	(3)	> 27.2	600V+GG435	old	1.8	0.77	0.168
GRB 050820A	2.61469	(4)	24.8	600B	old	2.6	0.86	0.147
GRB 050908	3.3467	(2)	27.7	600B	new	2.2	< 1.1	0.083
GRB 050922C	2.1992	(5)	> 26.3	600B	old	2.2	< 1.3	0.332
GRB 060115	3.5328	(2)	27.1	600V+GG435	old	2.1	1.23	0.447
GRB 060526	3.2213	(2); (9)	> 27.0	600B	new	2.2	0.93	0.221
GRB 060604	2.136	(6)	25.5	600B	new	1.7	< 1.1	0.142
GRB 060605	3.773	(7)	> 26.5	600V+GG435	new	1.4	< 1.5	0.164
GRB 060607A	3.0749	(2); (10)	> 27.9	300V	new	2.2	< 1.4	0.096
GRB 060707	3.4240	(2)	24.9	600V+GG435	new	1.4	1.02	0.071
GRB 060714	2.7108	(2)	26.4	300V	new	1.5	0.99	0.261
GRB 060908	1.8836	(11)	25.5	600B	new	1.5	< 0.9	0.099
GRB 061110B	3.4344	(2)	26.0	600B	new	2.2	< 1.0	0.127
GRB 070110	2.3521	(2)	25.0	600B	new	1.5	< 1.3	0.048
GRB 070506	2.3090	(2)	26.1	600B	new	1.5	< 1.2	0.130
GRB 070611	2.0394	(2)	> 27.0	600B	new	3.0	0.88	0.042
GRB 070721B	3.6298	(2)	27.5	300V	new	3.8	< 0.8	0.105
GRB 070802	2.4541	(2); (12)	25.1	600B	new	1.5	0.78	0.090

NOTE.— $R_{\text{host}}$  is the  $R$ -band total magnitude (or  $3\sigma$  upper limit) of the host galaxy (before correcting for Galactic extinction) from Malesani et al. (2012). CCD indicates which FORS1 CCD was used (cf. §2.3). The seeing was measured using a Gaussian fit to stars that happened to be in the slit in the combined spectrum. If no stars were available an upper limit on the seeing was set as the size of the smallest galaxy in the slit.  $A_V$  is the Galactic extinction in the  $V$ -band from Schlegel et al. (1998), as obtained from NED. The corresponding reddening is  $E(B - V) = A_V/3.315$ , and the Galactic extinction in the  $R$ -band is  $A_R = 2.673 E(B - V)$ .

References. — (1) Berger et al. (2005); (2) Fynbo et al. (2009); (3) Chen et al. (2005); (4) Prochaska et al. (2007); (5) Piranomonte et al. (2008); (6) Fynbo et al. (2009), but corrected for error (see text); (7) Ferrero et al. (2009); (8) Watson et al. (2006); (9) Thöne et al. (2010); (10) Fox et al. (2008); (11) Fynbo et al. (2009), but prompted by the  $\text{Ly}\alpha$  redshift from this work (see text); (12) Elíasdóttir et al. (2009).

prompted the discovery of a wavelength calibration error in the afterglow spectrum; the revised absorption-line redshift is  $z \approx 2.1361$ . We will adopt the value  $z = 2.136$ . GRB 060908 was originally included because it had an afterglow redshift of  $z = 2.43$  from Rol et al. (2006). Our spectroscopy (§2.3) gave a Ly $\alpha$  host emission redshift of  $z = 1.887$ . This prompted a re-analysis of the afterglow spectrum which did not find evidence for  $z = 2.43$  but which did find an afterglow redshift of  $z = 1.8836$  reported by Fynbo et al. (2009), matching our Ly $\alpha$  host redshift.

For the target selection for the TOUGH Ly $\alpha$  campaign there was no requirement that the hosts should be detected in the deep  $R$ -band imaging from the TOUGH imaging campaign (Malesani et al. 2012) or elsewhere. The statistics for the  $R$ -band imaging of the 20 observed systems with a secure redshift in the range 1.8–4.5 (Table 1) are: 14 hosts are detected in the  $R$ -band (with  $R$ -band magnitudes in the range 24.4 to 27.7) and 6 hosts are not detected down to a typical  $3\sigma$  limit of  $R = 27$ .

All observed bursts have a detected optical afterglow. This was not required, but is a consequence of the requirement of a known redshift before the end of the observing campaign. In all cases the redshift from the optical afterglow comes from interstellar absorption lines, both low-ionization metal lines (such as O I, Si II, and C II) and high-ionization lines (such as C IV and Si IV), providing a good estimate of the systemic redshift of the host galaxy. This is relevant for the interpretation of the velocity offset of the Ly $\alpha$  emission line with respect to the afterglow redshift (§3.2).

### 2.3. Observations

Spectroscopic observations were completed using the FORS1 spectrograph (cf. Appenzeller et al. 1998) on the Very Large Telescope (VLT) over the period May 2006 – May 2008 in service mode.

The detector system of FORS1 was changed in April 2007, i.e. during the observing campaign (cf. Table 1). The old system consisted of a single Tektronix CCD, providing a pixel scale of  $0.20'' \text{ px}^{-1}$ . The new system consists of two blue-optimized E2V CCDs, providing a pixel scale of  $0.25'' \text{ px}^{-1}$  when read out using the default  $2 \times 2$  binning as we did. The two CCDs are mounted

so that the small gap between them is in the spatial direction; the gap has no practical consequences for our program. Compared to the old detector system, the new detector system provides a larger recorded wavelength range, a higher efficiency below  $6000 \text{ \AA}$ , and suffers from fringing above  $6500 \text{ \AA}$ .

All targets were observed using a  $1.3''$  wide longslit. For most of the observing campaign, grisms 600B and 600V were used depending on the redshift of the target (see Table 1). Towards the end of the observing campaign the lower resolution but higher throughput 300V grism was used instead of 600B for some targets. The achieved wavelength range and spectral resolution for the different grisms and detector systems are listed in Table 2.

The targets, which were generally too faint to be seen in an acquisition image, were put in the slit using one of two methods, both involving a nearby reference star. Either the position angle of the slit was set so that the slit would go through the reference star and the target, or the reference star was put in the slit, after which an offset was applied to the telescope to put the target in the slit. The required position angle or offset was computed based on the  $R$ -band detection of the host or, for the hosts that were undetected or only marginally detected in our  $R$ -band host imaging, based on the position of the afterglow.

Each target was observed for a total exposure time of 1.4–3.8 hr (see Table 1), split into 4–8 individual exposures. The individual exposures were dithered along the slit. GRB 060714 was observed twice, since the first observation was obtained in poor transparency conditions. In the first observation the galaxy continuum was not detected, whereas in the second observation it was. The first observation was done using grism 600B, whereas the second observation was done using the more efficient grism 300V and with a slightly larger exposure time. In the analysis we will only use the data from the second observation.

Additionally, three bursts not in the TOUGH sample were observed. These are discussed separately in the Appendix.

TABLE 2  
WAVELENGTH RANGE AND SPECTRAL RESOLUTION

Grism+filter	Slit width (arcsec)	— Wavelength range —		FWHM (Å)	$R$	$c/R$ (km s <sup>-1</sup> )	— Dispersion —	
		old CCD (Å)	new CCDs (Å)				old CCD (Å px <sup>-1</sup> )	new CCDs (Å px <sup>-1</sup> )
600B	1.3	3300–5680	3030–6020	6.5	690	430	1.17	1.47
600V+GG435	1.3	4510–6850	4250–7190	6.2	920	330	1.15	1.44
300V	1.3	...	3000–8880 <sup>a</sup>	14.1	420	710	...	3.15
600R+GG435 <sup>b</sup>	1.3	5090–7220	...	6.5	950	320	1.05	...

<sup>a</sup>When grism 300V as here is used without an order sorter filter, a second order spectrum may be present for  $\lambda > 6600$  Å; this has no consequences for our program.

<sup>b</sup>Grism 600R is not relevant for the main part of this paper, only for the Appendix.

NOTE.—The FWHM values were measured from the [O I]λ5578 Å skyline in the combined science frames. The resolving power  $R = \lambda/\text{FWHM}$  values were computed at the central wavelength of the available wavelength range. Note that the listed values of FWHM and  $R$  only correspond to the spectral resolution of the obtained host galaxy spectrum if the observed spatial profile of the galaxy (i.e. the intrinsic profile convolved with the seeing) was flat over the slit. For a peaked spatial profile the obtained spectrum will have a better spectral resolution (i.e. smaller FWHM and larger  $R$ ).

## 2.4. Data reduction

Data reduction was performed mainly using IRAF<sup>8</sup>. The individual frames were bias subtracted and flat fielded. Cosmic ray events were removed using LACosmic (van Dokkum 2001). A 2D wavelength calibration was established for each grism and observing night (based on arc frames obtained the following day) and applied to the corresponding science frames. Vacuum wavelengths were used. The wavelength calibration was verified using the few strong skylines available, in particular [O I]λ5578.89. The shifts in pixels in the spatial direction between the individual science frames were computed in two ways: simply using the requested shifts stated in the so-called observation blocks (OBs), and using other objects (preferably stars) on the slits. The two derivations of shifts in all cases agreed to within 1 pixel ( $\approx 0.2''$ ).

The individual wavelength calibrated science frames were shifted in the spatial direction and

combined (averaged). Usually no weights were used, but for GRB 050820A and GRB 060604, the signal in other objects in the spectrum varied in a way indicating a variable transparency, and here weights were used. For GRB 050820A the weights were set to the flux of the reference star which was in the slit; the weights were in the range 0.25–1.00 when normalized to the largest value. For GRB 060604 no reference star was centered in the slit. Based on other objects in the slit, weights in the range 0.67–1.00 were assigned.

To represent the uncertainties for each pixel in the 2D science spectra, we calculated 2D sigma spectra based on photon noise and readout noise. The error (in ADU) in the given pixel is given by

$$\sigma = \sqrt{\frac{f}{g \cdot n} + \left(\frac{\text{RON}}{\sqrt{n}}\right)^2} \quad (1)$$

where  $f$  are the counts in ADU in the given pixel in the 2D science spectrum before sky subtraction,  $g$  is the gain (conversion factor) in  $e^-/\text{ADU}$  for a single image,  $n$  is the number of single images that were averaged in the combination, and RON is the read-out noise (in ADU) for a single image.

The spectra and sigma spectra were flux cali-

<sup>8</sup>IRAF is distributed by the National Optical Astronomy Observatories, which are operated by the Association of Universities for Research in Astronomy, Inc., under cooperative agreement with the National Science Foundation.

brated based on sensitivity functions derived from 30 standard star observations and reference data from Hamuy et al. (1992, 1994) and Oke (1990). The spectra and sigma spectra were corrected for atmospheric extinction. The extinction curve for La Silla was used (Tüg 1977; Schwarz & Melnick 1993), since no extinction curve was available for Paranal at the time of the reduction. A comparison between the La Silla curve and the Paranal FORS1 broad-band extinction coefficients (Patat 2003) shows a very good agreement (Milvang-Jensen et al. 2008).

The spectra and sigma spectra were finally corrected for Galactic extinction (Cardelli et al. 1989; O’Donnell 1994) using  $R_V = 3.1$ , with  $E(B - V)$  taken from Schlegel et al. (1998). Table 1 lists the used values.

It should be noted that the requested observing conditions were to have a transparency that was better than or equal to thin cirrus. This means that the spectra were not necessarily obtained under photometric conditions, and thus that some of the derived fluxes may be affected by thin cirrus. Any such effect is mitigated by the rescaling of the spectra based on the photometry (§3.1).

### 2.5. Subtraction of neighboring objects in the spectra

The spectra of two of the hosts were substantially contaminated by a neighboring object, which we fitted and subtracted in the 2D spectra. For GRB 070721B ( $z = 3.6$ ) a foreground galaxy ( $z = 3.1$ )  $1''$  away was fitted as a Gaussian in the spatial direction and a polynomial in the wavelength direction. For GRB 070802 the wings of a bright star in the slit  $18''$  away was fitted as a polynomial in both directions. The fits were performed using MPFIT (Markwardt 2009; Moré 1978). Figure 1 shows the spatial profiles before and after the subtraction of the neighboring objects. The subtraction makes the derived continuum flux densities of the hosts be 3.2 times (GRB 070721B) and 2.6 times (GRB 070802) smaller and much more in line with what the photometry predicts (cf. below). The EWs of Ly $\alpha$  (or upper limits thereof) become larger by the same factors. The Ly $\alpha$  fluxes, which are continuum-subtracted (cf. §3.1), are practically unaffected.

## 3. Results

### 3.1. Ly $\alpha$ detections and upper limits

We first describe the measurement of continuum flux densities in the spectra. We then compare these with the photometry and derive an average correction for slit loss and extraction aperture loss. We finally describe the measurement of Ly $\alpha$  fluxes and EWs from the spectra.

To measure the continuum flux density in the spectra, apertures on the blue and red side of Ly $\alpha$  were defined as follows. In rest-frame wavelength the apertures were  $175 \text{ \AA}$  wide and located such that a guard interval of  $\pm 6 \text{ \AA}$  (corresponding to  $\pm 1500 \text{ km s}^{-1}$ ) centered on Ly $\alpha$  placed at the afterglow redshift was excluded. In the spatial direction the continuum apertures coincided with the Ly $\alpha$  apertures (see below). The width of  $175 \text{ \AA}$  was the maximum value that was covered by all spectra, and this value also allowed an accurate measurement of the continuum flux density. Uncertainties on all measured fluxes and flux densities were calculated by propagating the individual uncertainties from the 2D sigma spectra (§2.4).

In Fig. 2(a) we compare the spectroscopy-based blue and red continuum flux densities. Of the 20 hosts in the sample, the red continuum is detected for 14 hosts, while the blue continuum is only detected for 9 hosts, all at  $\geq 3\sigma$  confidence; note that two of the blue non-detections are outside the plotted range in Fig. 2(a). One host (GRB 050908,  $z = 3.3$ , the magenta lower limit) is just above the  $3\sigma$  detection limit the blue ( $3.5\sigma$ ) but just below it in the red ( $2.2\sigma$ ), which is plausible given the redshift and the sensitivity curve of the used grism (600B). The seemingly discrepant point at  $z = 2.3$  (GRB 070506) is due to a time-variable pattern in the bias which we were unable to fully remove or quantify in terms of the error bars. This only has a noteworthy effect in the far blue where the sensitivity is very low and where the flux calibration therefore corresponds to a large amplification. This issue has no effect on the reported Ly $\alpha$  line properties, as we have adopted the continuum flux densities measured in the red window in the spectra as those used to subtract the (small) continuum contribution from the measured flux in the Ly $\alpha$  aperture and to calculate the EWs.

In order to investigate the absolute flux scale

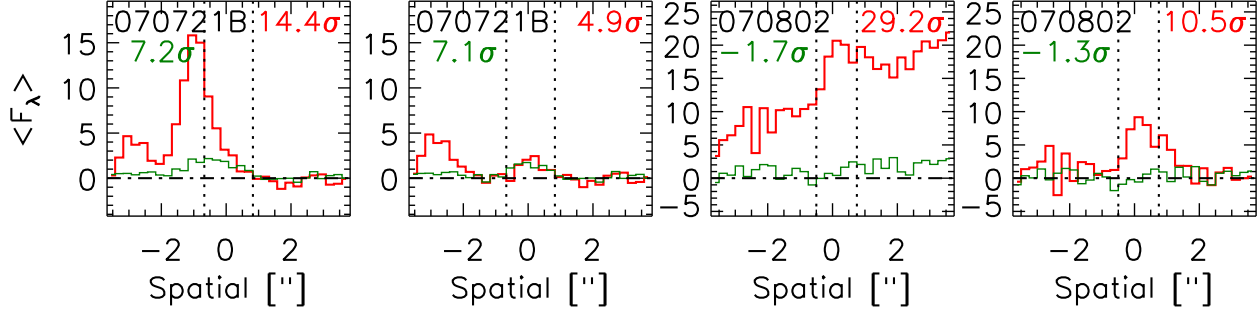


Fig. 1.— Spatial profiles of the GRB070721B and GRB070802 spectra before (1st panel) and after (2nd panel) a neighboring object was fitted and subtracted in the 2D spectrum. The red thick curve shows the continuum on the red side of Ly $\alpha$ , and the green curve shows Ly $\alpha$ . The subtraction of the neighboring object is evident from the red thick curve. The rest of the features of this plot are explained in the caption of Fig. 6.

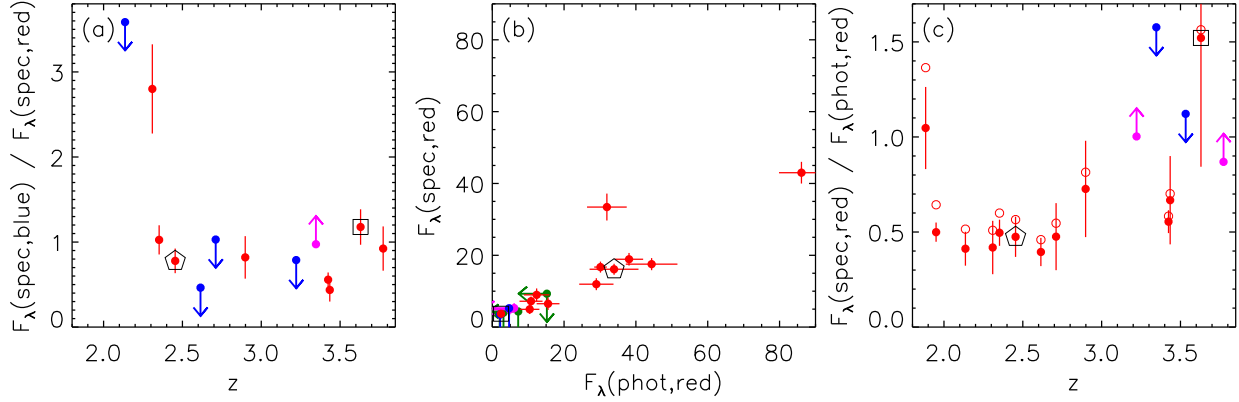


Fig. 2.— Comparison of continuum flux densities. Panel (a) compares the continuum flux densities measured in the spectra on the blue and red side of Ly $\alpha$ . Panels (b) and (c) compare the continuum flux densities measured in the spectra with those from the photometry (filled points:  $\beta = -1.5$ , open points [panel c only]:  $\beta = -1.0$ , cf. Eq. 4), both corresponding to the red side of Ly $\alpha$ . The units of the flux densities in panel (b) are  $10^{-20} \text{ erg cm}^{-2} \text{ s}^{-1} \text{ \AA}^{-1}$ . The blue and red windows are centered at 1122  $\text{\AA}$  and 1309  $\text{\AA}$  and have widths of 175  $\text{\AA}$ , all rest-frame. The two systems where a neighboring object was fitted and subtracted are marked: GRB070721B (box) and GRB070802 (pentagon). The discrepant point in panel (a) at  $z = 2.3$  is due to the blue window having very little signal and being dominated by a systematic error from a time-variable pattern in the bias, which has no effect on the derived Ly $\alpha$  properties presented in this paper as they are based on the continuum measured in the red window in the spectra (see text). The symbol colors in the panels simply reflect the symbol type: red = detections, blue = upper limits, magenta = lower limits, green = upper limits in both the  $x$  and  $y$  direction. The spectroscopic fluxes in this figure have not been multiplied by a factor of 2.0 to correct for slit losses and aperture losses.



of the fluxes and flux densities extracted from the spectra, we use our FORS2  $R$ -band host imaging (Malesani et al. 2012). The imaging was obtained largely under photometric conditions, and the photometry was calibrated using Landolt (1992). The derived magnitudes are total magnitudes, obtained either from using a large aperture, or from using a smaller aperture combined with an aperture correction. The correction was computed by analyzing the brighter host galaxies, and adopting as uncertainty the observed scatter.

Starting from the total  $R$ -band host magnitude  $R_{\text{host}}$ , we correct for Galactic extinction ( $A_R$ ) to obtain a flux density at the observed-frame wavelength of the  $R$ -band of

$$F_{\lambda,R} = f_{\lambda,\text{eff},R}^{\text{Vega}} \times 10^{-0.4(R_{\text{host}} - A_R)} , \quad (2)$$

where

$$f_{\lambda,\text{eff},R}^{\text{Vega}} = 2.15 \times 10^{-9} \text{ erg cm}^{-2} \text{ s}^{-1} \text{ \AA}^{-1} \quad (3)$$

is the conversion factor for Cousins  $R$  from Fukugita et al. (1995); practically the same factor would be obtained from Blanton & Roweis (2007)<sup>9</sup>. We then extrapolate this flux density from the effective wavelength of the  $R$ -band (6410  $\text{\AA}$ , Fukugita et al. 1995) to the observed-frame center wavelength of our red window,  $(1+z)1309 \text{ \AA}$ , by assuming an  $F_{\lambda} \propto \lambda^{\beta}$  spectrum, giving

$$F_{\lambda}(\text{phot, red}) = F_{\lambda,R} \times \left( \frac{(1+z)1309 \text{ \AA}}{6410 \text{ \AA}} \right)^{\beta} , \quad (4)$$

where  $\beta$  is the rest-frame UV spectral slope. We will use  $\beta = -1.5$  as a representative value (e.g., Shapley et al. 2003; Douglas et al. 2010; Finkelstein et al. 2011). Figure 2(c) shows the effect of  $\beta$  as function of redshift, since in addition to the adopted value of  $\beta = -1.5$  (filled points), the case of  $\beta = -1.0$  is illustrated (open points).

The spectroscopic flux densities show a good correlation with those from the photometry. This is shown in Fig. 2(b), where the two are plotted against each other, and in Fig. 2(c) where their ratio is plotted against redshift. 12 hosts have both a continuum detection (at  $3\sigma$ ) in the spectra on

the red side of  $\text{Ly}\alpha$  and a detection in the  $R$ -band host imaging (at  $2\sigma$ ). These hosts are shown as red points in Fig. 2(c). 2 hosts have a continuum detection in the spectra but not in the imaging; these are GRB 060526 and GRB 060605 and are shown as magenta lower limits in Fig. 2(c). 2 hosts conversely do not have a continuum detection in the spectra but have a detection in the imaging; these are GRB 050908 and GRB 060115 and are shown as blue upper limits in Fig. 2(c).

The ratio of spectroscopic to photometric flux density shown in Fig. 2(c) has a median value of 0.50 for the photometry extrapolated using  $\beta = -1.5$ . We attribute the fact that this median ratio is lower than 1 to slit losses (i.e. flux falling outside the slit) and extraction aperture losses (i.e. flux falling outside the used extraction apertures, as defined below), as well as possibly a small amount of thin cirrus affecting the observations (§2.4). We use this result to derive an approximate global scaling factor of  $1/0.50 = 2.0$  that we apply to all the flux calibrated science and sigma spectra (§2.4). This has the effect of making the derived  $\text{Ly}\alpha$  fluxes (or upper limits) and their uncertainties a factor of 2.0 larger, while the EWs are unaffected by this procedure<sup>10</sup>. This factor is used throughout the paper, except in Figs. 2 and 8.

The  $\text{Ly}\alpha$  fluxes were measured from the 2D spectra using a rectangular aperture defined in terms of  $v$ , the rest-frame velocity with respect to the afterglow redshift (cf. Table 1), and  $s$ , the spatial offset along the slit with respect to the afterglow position. If  $\text{Ly}\alpha$  was detected, the aperture was centered on the line and the width of the aperture was adjusted accordingly (as illustrated in the last 7 panels of Figs. 4–6). If  $\text{Ly}\alpha$  was not detected, an aperture of width  $900 \text{ km s}^{-1} \times 1.2''$  was used, centered at  $300 \text{ km s}^{-1}$  in  $v$  (a value typical for the detected lines, cf. §3.2) and at  $s = 0.0''$ . The aperture was defined in terms of integer pixels for simplicity. The centers and widths of the apertures are listed in Table 3. The width in  $v$  can be compared to the spectral resolution expressed as a rest-frame velocity,  $c/R$ , which is  $\lesssim 700 \text{ km s}^{-1}$ , cf. Table 2.

<sup>9</sup>For Bessel  $R$ , Blanton & Roweis (2007) find  $m_{\text{AB}} - m_{\text{Vega}} = 0.21 \text{ mag}$  and  $\lambda_{\text{eff}} = 6442 \text{ \AA}$ , which corresponds to a conversion factor (Eq. 3) of  $2.16 \times 10^{-9} \text{ erg cm}^{-2} \text{ s}^{-1} \text{ \AA}^{-1}$ .

<sup>10</sup>In reality the  $\text{Ly}\alpha$  EWs may in some cases be affected by slit loss, namely if the  $\text{Ly}\alpha$  and continuum emission differ in term of spatial distribution. We do not have the required  $\text{Ly}\alpha$  narrow-band imaging to investigate this issue.

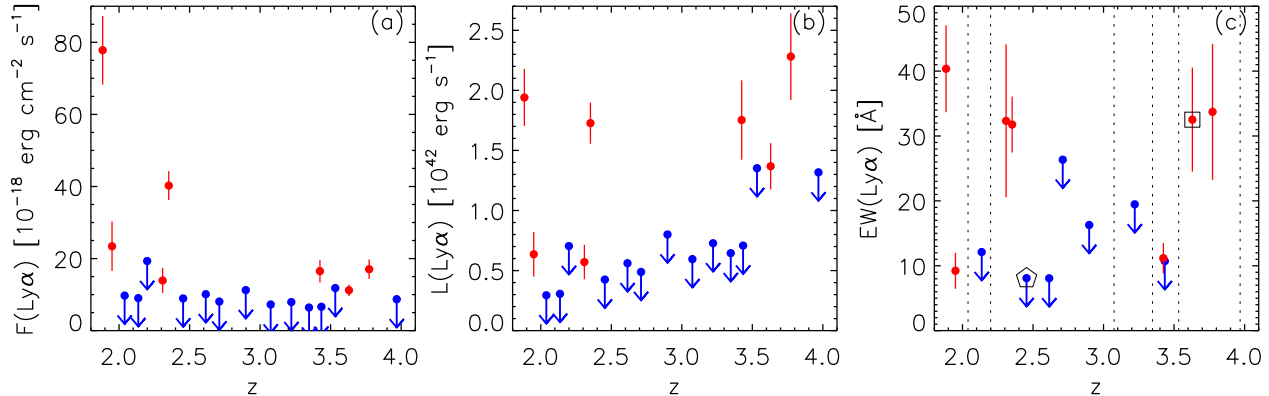


Fig. 3.—  $\text{Ly}\alpha$  fluxes, luminosities and (rest-frame) EWs for the 20 hosts in the sample. The dotted lines in panel (c) represent hosts for which no limit could be placed on the EW, due to detecting neither  $\text{Ly}\alpha$  nor the continuum in the spectra. The two systems where a neighboring object was fitted and subtracted are marked: GRB 070721B (box) and GRB 070802 (pentagon). The symbol colors simply reflect the symbol type: red = detections, blue = upper limits.

The fluxes within the  $\text{Ly}\alpha$  apertures in the 2D spectra were integrated by summing the flux densities (in  $\text{erg s}^{-1} \text{cm}^{-2} \text{\AA}^{-1}$ ) and multiplying by the spectral pixel size (in  $\text{\AA}$ ). Uncertainties were calculated by propagating the individual uncertainties from the 2D sigma spectra (§2.4). The continuum contribution was subtracted (if positive) and the errors propagated, to give the continuum-subtracted  $\text{Ly}\alpha$  fluxes listed in Table 3. If the  $\text{Ly}\alpha$  emission was not detected at  $3\sigma$  (with the  $\sigma$  being the uncertainty on the continuum-subtracted  $\text{Ly}\alpha$  flux), we give the  $3\sigma$  upper limit in the table.  $\text{Ly}\alpha$  emission was detected in 7 hosts out of 20: GRB 050315, GRB 060605, GRB 060707, GRB 060908, GRB 070110, GRB 070506, and GRB 070721B. Of these, only one was known to be a  $\text{Ly}\alpha$  emitter from the literature (GRB 070110, Fynbo et al. 2009).  $\text{Ly}\alpha$  emission was not detected at  $3\sigma$  for GRB 060714, only at  $2.5\sigma$ , but  $\text{Ly}\alpha$  emission was convincingly detected in the afterglow spectrum, cf. §3.3 below. Note that the 20 hosts in Figs. 4–6 are sorted by  $\text{Ly}\alpha$  detection significance, as listed on the panels.

Rest-frame EWs of  $\text{Ly}\alpha$  were calculated from the  $\text{Ly}\alpha$  fluxes and from the continuum flux densities measured in the spectra in a  $175 \text{\AA}$  [rest-frame] wide window on the red side of  $\text{Ly}\alpha$  centered at  $1309 \text{\AA}$  (cf. above), and the errors propagated. Throughout the remainder of this paper it is implicit that the EWs are rest-frame values.

The results are summarized in Fig. 3 which shows the  $\text{Ly}\alpha$  fluxes, luminosities and EWs (or upper limits in case of non-detections) versus redshift.

The spectra of the 20 systems are illustrated in three figures: (i) Smoothed 2D spectra centered on the  $\text{Ly}\alpha$  lines are shown in Fig. 4 with the used aperture indicated; (ii) 1D spectra (not smoothed) are shown in Fig. 5; and (iii) Spatial profiles (also not smoothed) are shown in Fig. 6.

### 3.2. Velocity offset between $\text{Ly}\alpha$ emission and low-ionization absorption lines in the afterglow spectra

For the 7 hosts with a  $\geq 3\sigma$  detection of  $\text{Ly}\alpha$  emission, the centroid in  $v$  within the  $\text{Ly}\alpha$  aperture was measured (see Table 3). Since the afterglow redshift defines the zero point of  $v$ , this velocity measurement is the velocity offset between the  $\text{Ly}\alpha$  emission centroid and low-ionization interstellar absorption in the GRB afterglow spectrum. A histogram of this offset for the 7 hosts is given in Fig. 7. The range is  $200\text{--}700 \text{ km s}^{-1}$ , consistent with the few values for GRB hosts reported in the literature (cf. Table 5). The histogram resembles the distribution of velocity offsets between  $\text{Ly}\alpha$  emission and low-ionization interstellar absorption in LBGs (Adelberger et al. 2003; Shapley et al. 2003; see also Pettini et al. 2000). The distribution is also in agreement with the velocity offsets for two  $\text{Ly}\alpha$ -selected galaxies re-

TABLE 3  
 LY $\alpha$  MEASUREMENTS FROM THE SPECTRA

Name	Ly $\alpha$ aperture				$F(\text{Ly}\alpha)$	$L(\text{Ly}\alpha)$	$F_\lambda(\text{cont.})$	EW(Ly $\alpha$ )	$v(\text{Ly}\alpha)$
	c( $v$ )	c( $s$ )	w( $v$ )	w( $s$ )					
(1)	(2)	(3)	(4)	(5)	(6)	(7)	(8)	(9)	(10)
GRB 050315	290	0.08	1102	1.50	$23.4 \pm 6.8$	$0.64 \pm 0.19$	$86.0 \pm 6.0$	$9.2 \pm 2.8$	$283 \pm 62$
GRB 050401	326	-0.10	888	1.20	< 11.2	< 0.80	$18.0 \pm 3.6$	< 16.3	...
GRB 050730	302	-0.04	856	1.20	< 8.7	< 1.32	< 8.0	...	...
GRB 050820A	309	0.06	878	1.20	< 10.1	< 0.56	$35.1 \pm 3.4$	< 8.1	...
GRB 050908	281	-0.08	914	1.25	< 6.4	< 0.64	< 7.0	...	...
GRB 050922C	342	-0.10	902	1.20	< 19.3	< 0.70	< 18.6	...	...
GRB 060115	303	-0.10	938	1.20	< 11.8	< 1.35	< 10.5	...	...
GRB 060526	294	0.00	941	1.25	< 7.9	< 0.73	$9.8 \pm 2.8$	< 19.5	...
GRB 060604	307	0.00	806	1.25	< 9.0	< 0.31	$23.9 \pm 3.3$	< 12.1	...
GRB 060605	564	-0.25	594	1.25	$17.0 \pm 2.7$	$2.28 \pm 0.36$	$10.6 \pm 2.8$	$33.7 \pm 10.5$	$620 \pm 26$
GRB 060607A	337	-0.05	953	1.25	< 7.3	< 0.60	< 7.3	...	...
GRB 060707	788	-1.10	961	2.00	$16.5 \pm 3.1$	$1.75 \pm 0.33$	$33.4 \pm 3.1$	$11.2 \pm 2.3$	$742 \pm 38$
GRB 060714	373	-0.05	837	1.25	< 8.1	< 0.49	$9.9 \pm 2.6$	< 26.3	...
GRB 060908	372	1.00	1002	1.75	$77.8 \pm 9.5$	$1.94 \pm 0.24$	$66.8 \pm 7.5$	$40.4 \pm 6.7$	$347 \pm 31$
GRB 061110B	294	0.12	896	1.25	< 6.6	< 0.71	$14.4 \pm 2.6$	< 10.7	...
GRB 070110	345	-0.22	1078	1.75	$40.2 \pm 4.0$	$1.73 \pm 0.17$	$37.8 \pm 3.5$	$31.8 \pm 4.3$	$358 \pm 26$
GRB 070506	379	-0.12	983	1.25	$13.9 \pm 3.5$	$0.57 \pm 0.14$	$13.0 \pm 3.5$	$32.3 \pm 11.8$	$360 \pm 62$
GRB 070611	319	-0.05	951	1.25	< 9.7	< 0.29	< 8.7	...	...
GRB 070721B	271	0.08	839	1.50	$11.2 \pm 1.6$	$1.37 \pm 0.19$	$7.4 \pm 1.5^a$	$32.5 \pm 8.0^a$	$212 \pm 31$
GRB 070802	321	0.12	941	1.25	< 8.9	< 0.43	$32.2 \pm 3.1^a$	< 8.1 <sup>a</sup>	...

<sup>a</sup>The listed error reflects the random error only. A systematic error due to the fitting and subtraction of a neighboring object is likely present.

NOTE.—Columns (2)–(5) define the aperture in the 2D spectrum within which the Ly $\alpha$  flux was measured. Specifically, the columns give the center (c) and width (w) of the aperture in terms of  $v$  (in  $\text{km s}^{-1}$ ), the rest-frame velocity with respect to the afterglow redshift (cf. Table 1), and  $s$  (in arcsec), the spatial offset along the slit with respect to the afterglow position. The subsequent columns are: (6)  $F(\text{Ly}\alpha)$ , the Ly $\alpha$  emission line flux, in units of  $10^{-18} \text{ erg cm}^{-2} \text{ s}^{-1}$ ; (7)  $L(\text{Ly}\alpha)$ , the Ly $\alpha$  luminosity, in units of  $10^{42} \text{ erg s}^{-1}$ ; (8)  $F_\lambda(\text{cont.})$ , the continuum flux density measured in a  $175 \text{ \AA}$  rest-frame wide aperture (centered at  $1309 \text{ \AA}$ ) on the red side of Ly $\alpha$ , in units of  $10^{-20} \text{ erg cm}^{-2} \text{ s}^{-1} \text{ \AA}^{-1}$ ; (9) EW(Ly $\alpha$ ), the rest-frame Ly $\alpha$  equivalent width, in  $\text{\AA}$ ; (10)  $v(\text{Ly}\alpha)$ , the rest-frame velocity of the Ly $\alpha$  emission line with respect to the afterglow redshift, i.e. the centroid of  $v$  within the aperture, in  $\text{km s}^{-1}$ . The listed error on  $v(\text{Ly}\alpha)$  is only based on the errors on the fluxes within the aperture, and does not include the error on the afterglow redshift. All upper limits are  $3\sigma$ . The flux calibrated science spectra and their uncertainties (sigma spectra) have been multiplied by a factor of 2.0 to correct for slit loss and aperture loss (§3.1). This has made all the numbers in columns (6), (7) and (8) be larger by this factor.

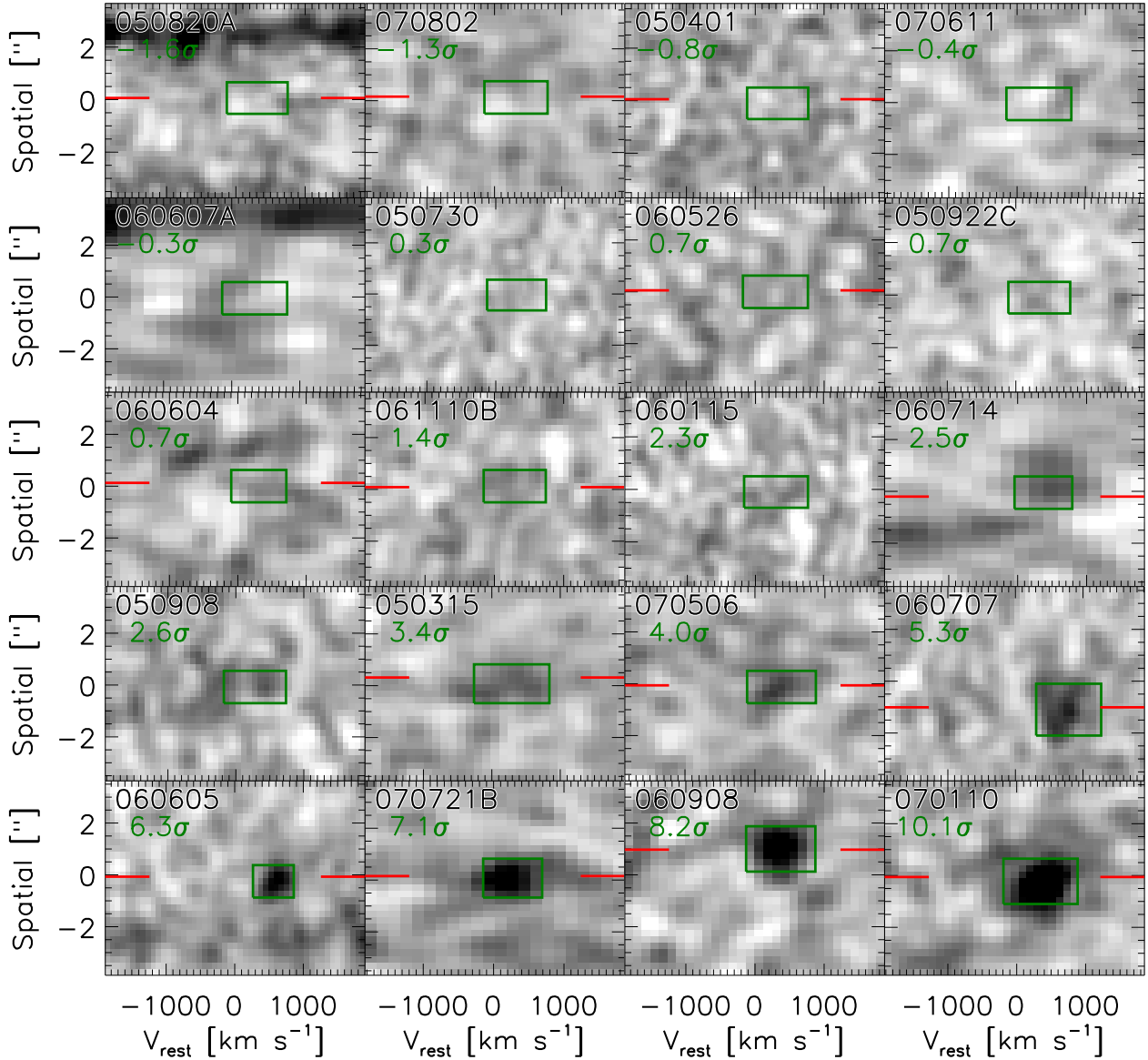


Fig. 4.— The obtained 2D spectra, centered on where Ly $\alpha$  is expected. The zero point for the rest-frame velocity is defined by the afterglow redshift listed in Table 1. The zero point for the spatial (angular) position corresponds to the afterglow position. The shown sections have size  $3800 \text{ km s}^{-1} \times 7.5''$ . The spectra have been smoothed by a Gaussian with FWHM = 3 px. The intensity cuts are the same for all the panels, in units of the noise in the given spectrum, allowing a visual comparison of the significance of the features in the different panels. The green rectangle marks the aperture within which the Ly $\alpha$  flux and its uncertainty are measured; the aperture centers and widths are listed in Table 3. On the panels is stated by how many sigma Ly $\alpha$  is detected; the panels are sorted by this. The red horizontal lines indicate where the continuum (if detected at  $\geq 3\sigma$ ) is located, as defined by the spatial centroid in the aperture in which the continuum is measured, cf. Fig. 6.

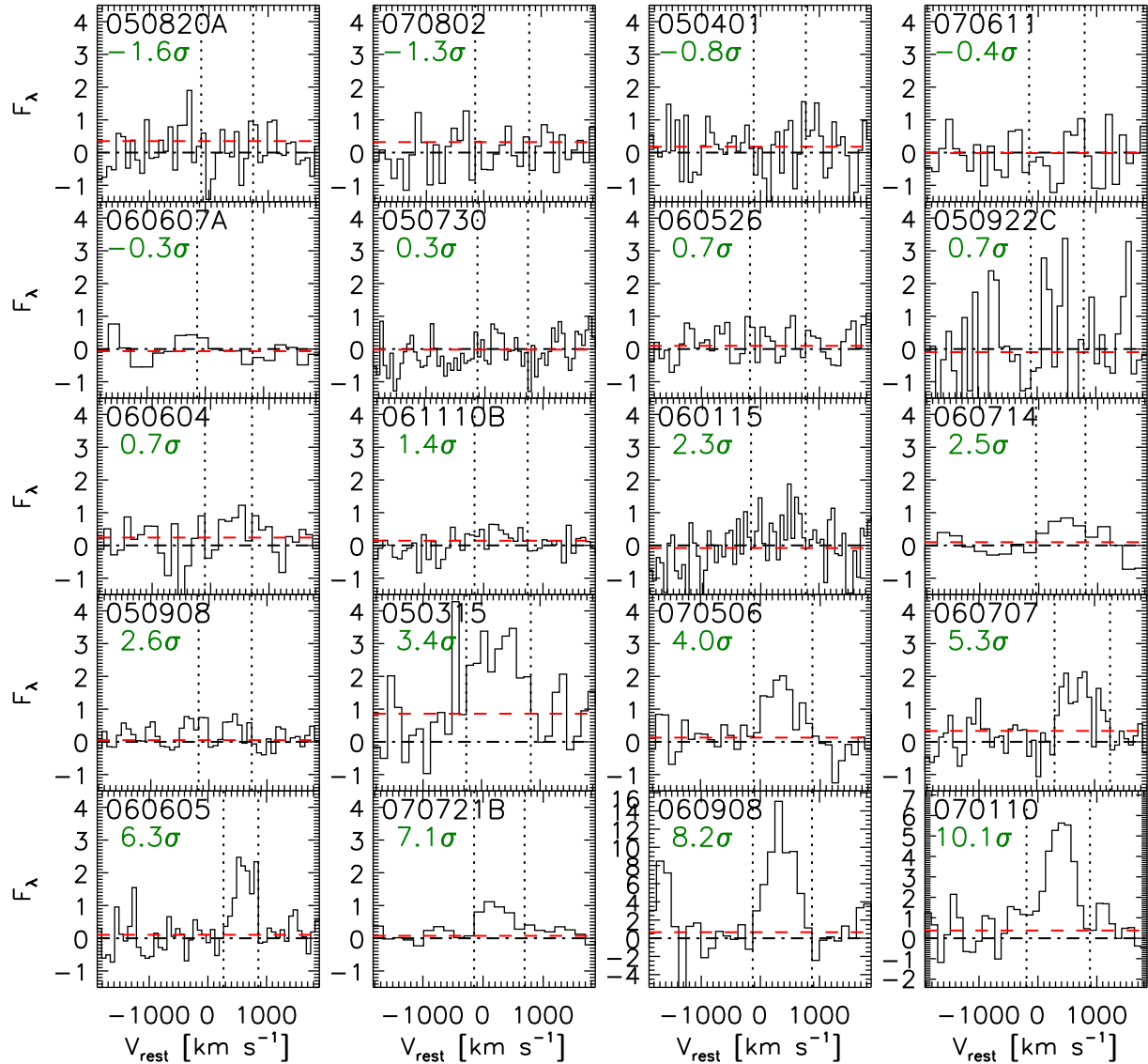


Fig. 5.— 1D spectra, derived by a straight sum over the spatial aperture (cf. Table 3). The flux densities  $F_\lambda$  are in units of  $10^{-18} \text{ erg s}^{-1} \text{ cm}^{-2} \text{ \AA}^{-1}$ . No smoothing has been applied. The detection significance of the Ly $\alpha$  emission line is given on the panel; the panels are sorted by this. The vertical dotted lines mark the velocity limits of the Ly $\alpha$  aperture, cf. Table 3. The horizontal dot-dashed (black) line simply indicates zero, while the horizontal dashed (red) line indicates the continuum, measured as the mean level in a 175  $\text{\AA}$  rest-frame wide window on the red side of Ly $\alpha$ . The plotted range in velocity corresponds to the range of the 2D spectra shown in Fig. 4.

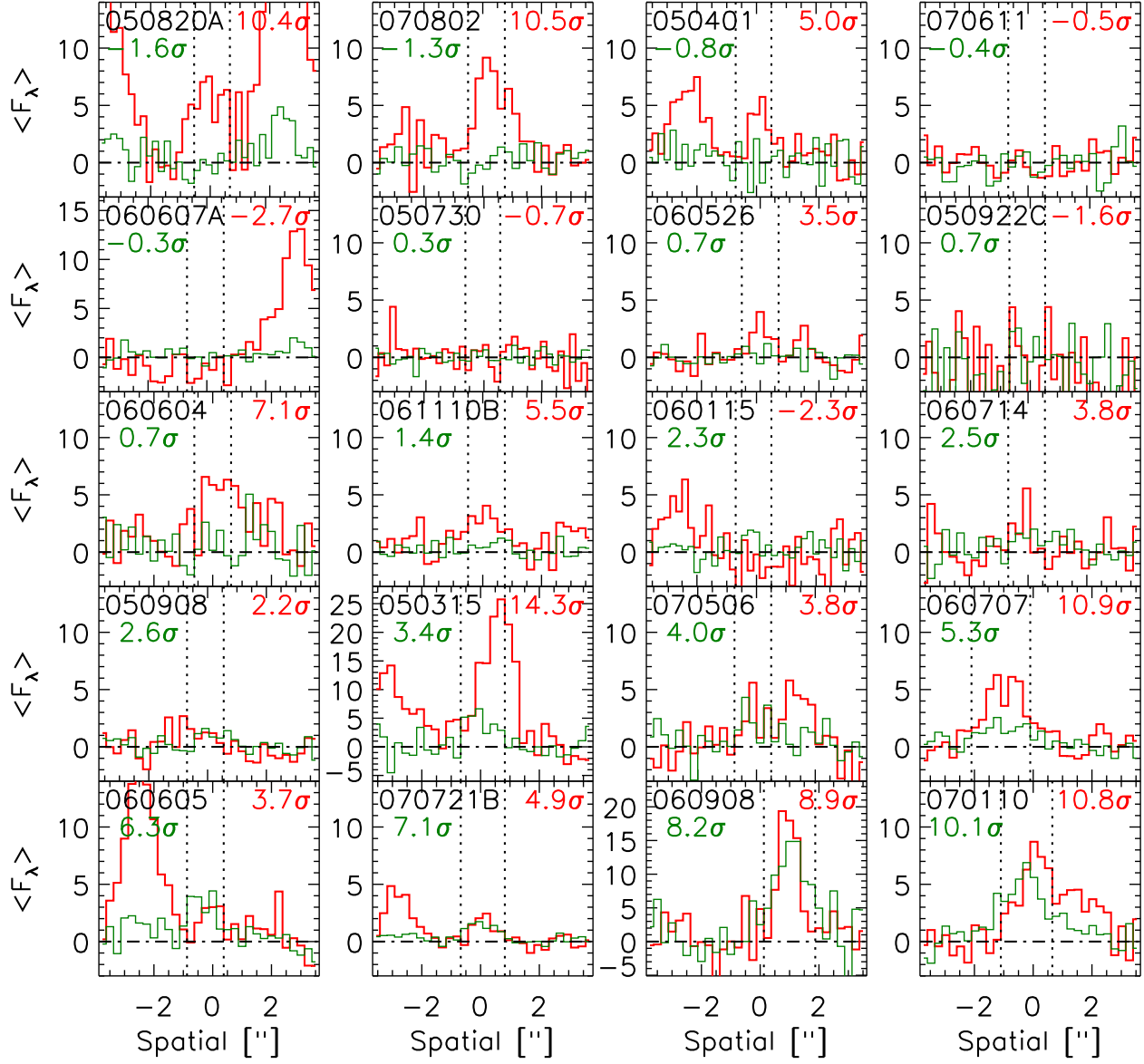


Fig. 6.— Spatial profiles, i.e. the flux densities averaged over a given wavelength range versus spatial coordinate in the 2D spectrum. Red thick curve:  $\langle F_\lambda \rangle$  calculated over the  $175 \text{ \AA}$  rest-frame wide continuum window on the red side of  $\text{Ly}\alpha$ , in units of  $10^{-20} \text{ erg s}^{-1} \text{ cm}^{-2} \text{ \AA}^{-1}$ . Green curve:  $\langle F_\lambda \rangle$  calculated over the wavelength range of the  $\text{Ly}\alpha$  aperture, in units of  $10^{-19} \text{ erg s}^{-1} \text{ cm}^{-2} \text{ \AA}^{-1}$ . No smoothing has been applied. The detection significance of the continuum in the above-mentioned red window is given on the right hand side of the panel in red, and the detection significance of the  $\text{Ly}\alpha$  emission line is given on the left hand side of the panel in green. The vertical dotted lines mark the spatial limits of the  $\text{Ly}\alpha$  aperture, cf. Table 3. The plotted range in spatial coordinate corresponds to the range of the 2D spectra shown in Fig. 4. The panels are sorted by  $\text{Ly}\alpha$  detection significance.

ported by McLinden et al. (2011) using the [O III] emission line to define the systemic velocity. It should be noted that the assumption that the afterglow redshift provides the systemic velocity is only valid on average (over a sample of hosts). For individual hosts the GRB sightline may probe a region of the host that has a non-zero velocity due to the internal kinematics of the galaxy (e.g. rotation). This cannot be a large effect, since otherwise the measured velocity offsets of Ly $\alpha$  (Fig. 7) would not all have the same sign.

It should be noted that what we measure is simply the centroid of the Ly $\alpha$  emission line in our GRB host spectra, which may not be identical to the peak of the line if the line is asymmetrical. Our spectra (Fig. 5) do not have sufficient spectral resolution or S/N to investigate this issue.

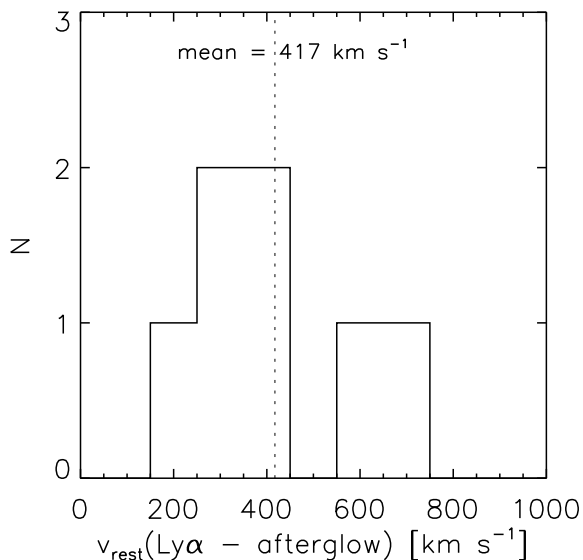


Fig. 7.— Distribution of velocity offsets between the centroid of the Ly $\alpha$  emission in the GRB host spectrum and low-ionization interstellar absorption lines in the GRB afterglow spectrum.

The origin of the offset is most likely a combination of radiative transfer of the resonantly scattered Ly $\alpha$  photons and a star-formation driven outflow from the host galaxy (for a full discussion of these effects we refer to Fynbo et al. 2010, their §4.3). It should be emphasized that the velocities presented in Table 3 and Fig. 7 simply represent the centroid of the Ly $\alpha$  line in the spectrum (with respect to the afterglow redshift);

they do not directly translate into outflow velocities. In the outflow scenario several factors affect the observed redwards shift of the Ly $\alpha$  velocity centroid with respect to the systemic velocity. High column densities and (to a lesser extent) low temperatures push the Ly $\alpha$  peak further from the systemic velocity (Harrington 1973). The velocity shift also increases with increasing outflow velocities, up to  $\sim 10^3$  km s<sup>-1</sup>, where the peak starts to drift back toward the systemic velocity (e.g. Verhamme et al. 2006). On the other hand, if dust is present, preferentially the wings of the line are removed, effectively reducing the shift (Laursen et al. 2009). This effect is stronger the more homogeneous the medium is, since clumpiness of the gas and dust facilitates the escape of Ly $\alpha$  photons (Neufeld 1991; Hansen & Oh 2006).

### 3.3. Ly $\alpha$ emission comparison: host and afterglow spectra

For three of the hosts in the sample Ly $\alpha$  emission was detected directly in the afterglow spectra: GRB 060714 (Jakobsson et al. 2006b), GRB 070110 (Fynbo et al. 2009), and also marginally in GRB 070721B (Fynbo et al. 2009). Figure 8 compares the spectra. For GRB 070110 and GRB 070721B the Ly $\alpha$  flux measured from the afterglow and host spectroscopy is consistent within the errors (at 2 sigma). However, for GRB 060714 there is a significant difference, with the Ly $\alpha$  flux from the afterglow spectrum being almost a factor of 4 larger than in the host spectrum reported here. In the afterglow spectrum the Ly $\alpha$  emission appears to be very extended both spatially and in velocity space. In addition, the position angles of the two observations are nearly perpendicular (0° east of north for the afterglow spectrum and 116° for the host galaxy spectrum). Hence, we suspect the cause of the difference is a higher slit loss in the host galaxy spectrum. It is possible that other of the 12 hosts where we do not detect Ly $\alpha$  emission at  $\geq 3\sigma$  actually would have been detected as Ly $\alpha$  emitters had we used a slit at a different position angle or a wider slit.

## 4. Discussion and summary

In this work we have carried out a systematic search for Ly $\alpha$  photons from GRB host galaxies selected from the larger well-defined TOUGH

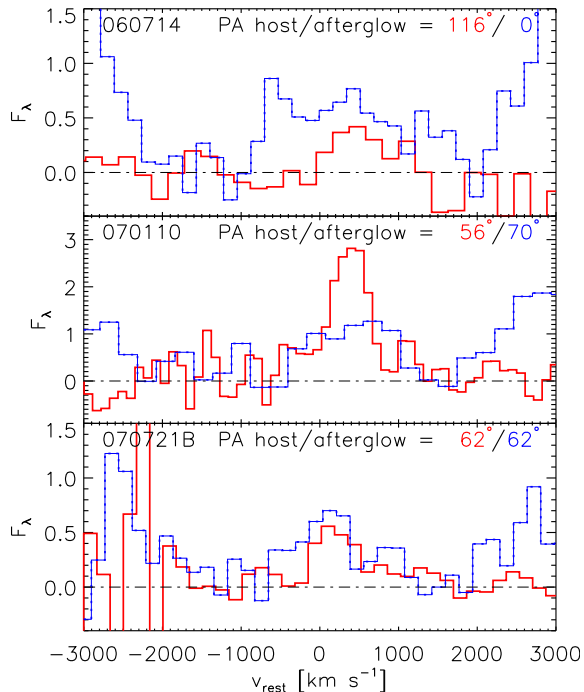


Fig. 8.— Comparison of host spectra (red solid lines) with afterglow spectra (blue dotted+solid lines). The three GRBs shown are those for which Ly $\alpha$  emission was detected in the afterglow spectrum superimposed on the damped Ly $\alpha$  absorption trough. The position angle (PA) of the slit is given on the panels; note the large PA difference between host and afterglow spectroscopy for GRB 060714. The spectra have been corrected for Galactic extinction.  $F_\lambda$  is given in units of  $10^{-18} \text{ erg cm}^{-2} \text{ s}^{-1} \text{ \AA}^{-1}$ . In the comparison for GRB 070721B it should be noted that only the host spectrum has had a neighboring galaxy subtracted (cf. §3.1), a procedure that decreases the overall flux level by about 0.1 in the plotted units. The afterglow spectra were taken from Jakobsson et al. (2006b) [GRB 060714] and Fynbo et al. (2009) [GRB 070110 and GRB 070721B]. None of the spectra in this figure have been corrected for slit losses or aperture losses.

sample of such galaxies presented in Hjorth et al. (2012). Unlike previous studies (cf. Fynbo et al. 2003) we find that Ly $\alpha$  emission is not ubiquitous among GRB host galaxies. Of the 20 host galaxies studied here we detect (at  $3\sigma$ ) Ly $\alpha$  emission from 7 of them (with the Ly $\alpha$  [rest-frame] EW in the range 9–40 Å), derive  $3\sigma$  upper limits on the Ly $\alpha$  EW for 7 of them (in the range 8–26 Å), while we obtain no constraints on the Ly $\alpha$  EW for the last 6 hosts (due to neither detecting the continuum nor Ly $\alpha$  emission in the spectra, both at  $3\sigma$ ), cf. Table 3. Out of the 14 hosts with either a Ly $\alpha$  EW or an upper limit on the EW, 8 hosts have Ly $\alpha$  EW less than 20 Å (rest-frame), which is the typical limit in narrow-band surveys for Ly $\alpha$  emitters. For the 7 detections, the measured EWs in the range 9–40 Å are low compared to the distribution of EWs found for narrow-band selected galaxies at similar redshifts (Gronwall et al. 2007; Grove et al. 2009; Nilsson et al. 2009).

The Ly $\alpha$  luminosities for the 7 GRB hosts with detected Ly $\alpha$  emission are in the range  $(0.6\text{--}2.3) \times 10^{42} \text{ erg s}^{-1}$ . Such fairly low Ly $\alpha$  luminosities are only probed by a few studies of Ly $\alpha$  emitting galaxies, e.g. Rauch et al. (2008); Grove et al. (2009); Cassata et al. (2011). The Ly $\alpha$  luminosity can be translated into a star-formation rate (SFR), assuming no dust extinction, as

$$\text{SFR} = \frac{L(\text{Ly}\alpha)}{1.1 \times 10^{42} \text{ erg s}^{-1}} M_\odot \text{ yr}^{-1}, \quad (5)$$

using the relation between SFR and  $L(\text{H}\alpha)$  from Kennicutt (1998) and the case B recombination ratio  $L(\text{Ly}\alpha)/L(\text{H}\alpha) = 8.7$  (Brocklehurst 1971). The observed range in Ly $\alpha$  luminosity for the 7 detections would translate into a range in SFR of  $0.6\text{--}2.1 M_\odot \text{ yr}^{-1}$ , but the assumption of no dust extinction is likely not always correct, as illustrated by the trends of Ly $\alpha$  luminosity and EW with afterglow spectral index discussed in §4.2. If dust is present then Eq. (5) provides a lower limit of the SFR.

#### 4.1. Comparison with LBGs

Lyman-break selection and GRB selection are complementary methods to identify samples of galaxies at high redshift. In this section and in Fig. 9 we carry out a comparison of the LBGs from Shapley et al. (2003) with the GRB host galaxies from this work.



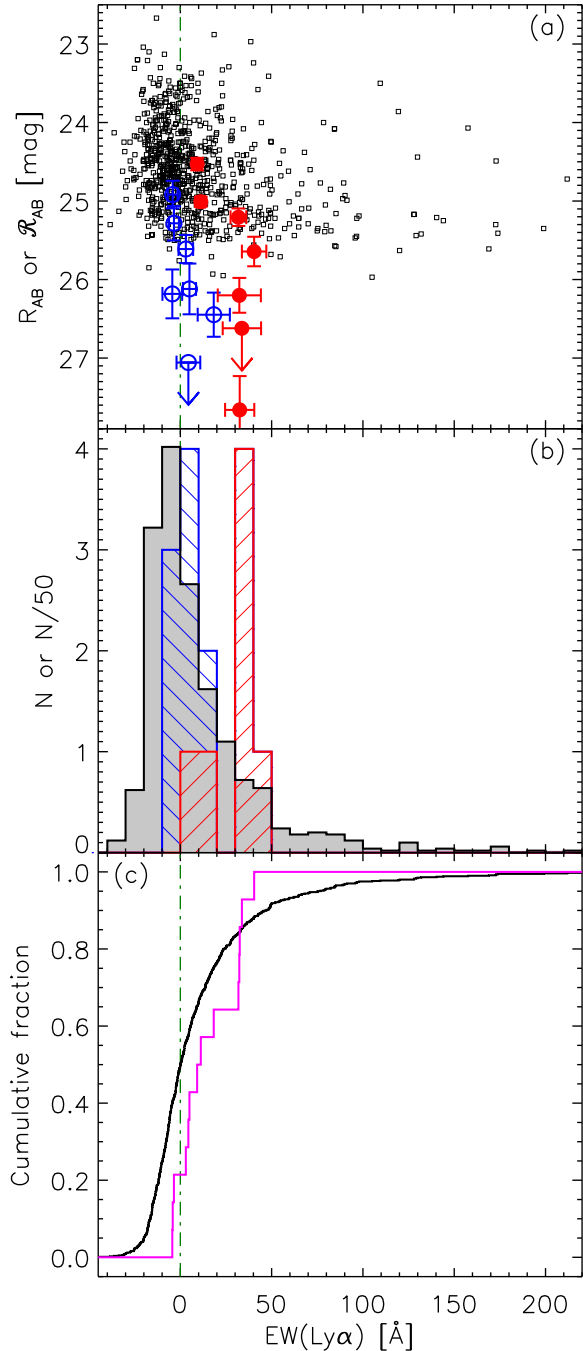


Fig. 9.— Comparison of Ly $\alpha$  EWs between the LBGs from Shapley et al. (2003) and the GRB host galaxies from this work. Small black points and grey/black histogram: LBGs ( $N = 803$ ). Other points: GRB host galaxies ( $N = 14$ ), in (a) and (b) split into galaxies with detected Ly $\alpha$  emission (red filled circles and histogram) and without (blue open circles and histogram).

The 20 GRB host galaxies from this work fall into 3 categories. For 6 galaxies we detected neither the continuum nor Ly $\alpha$  emission in the spectra, and these galaxies are omitted from the analysis. For 7 galaxies we detected both the continuum and Ly $\alpha$  emission in the spectra, and for these we use the Ly $\alpha$  EWs reported in Table 3. For another 7 galaxies we detected the continuum but not Ly $\alpha$  emission in the spectra. In Table 3 and the rest of the paper we have reported the  $3\sigma$  upper limits on the Ly $\alpha$  EWs. An example is GRB 061110B where the measured [rest-frame] EW is  $5.0 \pm 3.6 \text{ \AA}$ , which we replaced by the  $3\sigma$  upper limit of EW  $< 10.7 \text{ \AA}$ . This procedure implicitly assumes that Ly $\alpha$  can only be in emission. However, the LBGs from Shapley et al. (2003) often show significant Ly $\alpha$  absorption (negative EWs), so in order to make a fair comparison with that sample, we use the measured EWs also for the 7 GRB host galaxies without detected Ly $\alpha$  emission<sup>11</sup>.

Figure 9(a) shows apparent  $R$ -band magnitude<sup>12</sup> versus Ly $\alpha$  EW. The 803 LBGs are shown as small black open squares. The 7 GRB host galaxies with Ly $\alpha$  emission detected at  $3\sigma$  are shown as red filled circles, and the 7 GRB host galaxies without such detected Ly $\alpha$  emission are shown as blue open circles. The plot shows that the GRB hosts from this work typically are fainter than the LBGs from Shapley et al. (2003). This is also the case for the luminosities, since the redshift distributions of the two samples are fairly similar: LBGs:  $\langle z \rangle = 3.0$ ,  $\text{sd} = 0.3$ ; GRB host galaxies:  $\langle z \rangle = 2.8$ ,  $\text{sd} = 0.6$  (with  $\text{sd}$  being the standard deviation). It is tempting to define a faint subset of the LBG sample that is better matched to our sample, but Shapley et al. (2003) conclude that the redshift incompleteness at fainter magnitudes (say fainter than  $\mathcal{R} \approx 24.5$ , cf. Fig. 7 in Shapley et al. 2003) is likely such that preferentially galaxies without (strong) Ly $\alpha$  emission are missing. This might argue for only comparing our GRB hosts with a *bright* LBG subsample, but then the luminosity difference would

<sup>11</sup>These EWs are: GRB 050401:  $-4.4 \pm 5.4 \text{ \AA}$ ; GRB 050820A:  $-4.2 \pm 2.7 \text{ \AA}$ ; GRB 060526:  $4.4 \pm 6.5 \text{ \AA}$ ; GRB 060604:  $3.0 \pm 4.0 \text{ \AA}$ ; GRB 060714:  $18.3 \pm 8.8 \text{ \AA}$ ; GRB 061110B:  $5.0 \pm 3.6 \text{ \AA}$ ; and GRB 070802:  $-3.5 \pm 2.7 \text{ \AA}$ .

<sup>12</sup>The apparent magnitudes in Fig. 9(a) are on the AB system and have been corrected for Galactic extinction. The filter used for the LBGs from Shapley et al. (2003) is  $\mathcal{R}$ , see Steidel & Hamilton (1993).

be substantial. We will therefore simply use the full Shapley et al. (2003) for comparison with our GRB host sample.

Figure 9(b) shows histograms of the EWs: grey filled histogram: LBGs; hatched histograms: GRB hosts galaxies, with blue and red having the same meaning as in panel (a). The LBG histogram has been scaled down by a factor of 50, but is otherwise identical to Fig. 8 in Shapley et al. (2003).

Figure 9(c) shows the cumulative EW distributions: smooth black curve: LBGs; jagged magenta curve: the 14 GRB host galaxies. A Kolmogorov–Smirnov (K–S) test (e.g. Press et al. 1992) gives a 1.7% probability that the two samples are drawn from the same parent distribution. In other words, we detect a difference at 98.3% confidence between the two samples. This result is driven by the lack of GRB host galaxies with substantial Ly $\alpha$  absorption (i.e. with EWs below  $-5 \text{ \AA}$ ).

Fynbo et al. (2003) also found a significant difference (99.8% confidence) between the EWs of 5 pre-*Swift* GRB host galaxies and an approximation of the Shapley et al. (2003) distribution. If we use our updated compilation of the EWs for these 5 pre-*Swift* hosts and carry out a K–S test against the Shapley et al. (2003) sample, we get a similar result, namely a difference that is significant at 99.2% confidence. We compare the pre-*Swift* sample with the sample from this work in §4.2.

#### 4.2. The relation between afterglow spectral index and host Ly $\alpha$ emission, and comparison with pre-*Swift* studies

Remarkably, substantially larger EWs were found in the previous, pre-*Swift* studies of Ly $\alpha$  emission from GRB hosts despite the fact that these studies targeted a much smaller sample (Fynbo et al. 2003, and references therein). Our updated compilation of the EWs for the 5 pre-*Swift* hosts studied by Fynbo et al. (2003) is given in the first 5 rows of Table 5; the 3 large values around 70–100  $\text{\AA}$  are noteworthy. A K–S test comparing the EWs of the pre-*Swift* sample ( $N = 5$ ) with the sample from this work ( $N = 14$ , cf. §4.1) gives an 8% probability that the two samples are drawn from the same parent distribution. This is marginal evidence for a difference. This difference could therefore be a chance effect, but another

plausible explanation is different biases in the two samples.

The present sample is based on an underlying X–ray selected sample of 69 bursts (the TOUGH sample, see §2.1 and Hjorth et al. 2012) which is nearly unbiased. The sample of 20 bursts followed up for Ly $\alpha$  spectroscopy in this work (i.e. those with a known afterglow redshift in the range 1.8–4.5) is biased since an optical afterglow was *de facto* required, and since some bursts in the TOUGH sample were without a determined redshift at the time of the target selection for the Ly $\alpha$  spectroscopy and thus could be in the targeted redshift range of 1.8–4.5 (indeed, 7 of these bursts were recently found to be at  $z = 1.8$ –4.5 from X–shooter host spectroscopy, see Krühler et al. 2012 and below, while 20 of the TOUGH bursts still do not have a determined redshift, cf. §2.2). The pre-*Swift* sample of 5 bursts (Fynbo et al. 2003, and references therein) is even more biased towards relatively bright optical afterglows due to the larger times to localize the burst and larger localization uncertainties (see also Kann et al. 2010). This is shown in Fig. 10(a), where we plot the afterglow *R*–band magnitude at 12 hr after the burst (see Table 4) versus redshift for the pre-*Swift* sample (open green stars) and the *Swift* sample from this work (other symbols). In panel (b) we plot EW(Ly $\alpha$ ) (detections, and for our sample also upper limits) versus afterglow magnitude. Comparing the two samples suggests that the larger Ly $\alpha$  EWs for the pre-*Swift* sample is related to brighter afterglows, which in turn could be related to galaxies having less dust. On the other hand, within the sample from this work there is no evidence for a correlation between Ly $\alpha$  EW and afterglow magnitude.

To further examine the role of dust we turn to the afterglow spectral index  $\beta_{\text{OX}}$ , defined by

$$\beta_{\text{OX}} = \frac{\log [F_{\nu}(\nu_{\text{opt}})/F_{\nu}(\nu_{\text{X}})]}{\log [\nu_{\text{X}}/\nu_{\text{opt}}]}, \quad (6)$$

where  $F_{\nu}$  is the flux density of the afterglow and where  $\nu_{\text{opt}}$  and  $\nu_{\text{X}}$  are representative center frequencies (pivotal frequencies) of the optical and X–ray bands, respectively. If  $F_{\nu}$  were a single power-law between  $\nu_{\text{opt}}$  and  $\nu_{\text{X}}$  it would have the form  $F_{\nu} \propto \nu^{-\beta_{\text{OX}}}$ . A low value of  $\beta_{\text{OX}}$  indicates suppression of the optical emission compared to the X–ray flux. For low-redshift events (e.g. for

TABLE 4  
AFTERGLOW  $R$ -BAND MAGNITUDES AT 12 HR AFTER THE BURST — THE 5 PRE-*Swift*  $\text{Ly}\alpha$  EMITTERS  
AND THE 20 HOSTS FROM THIS WORK

Name	EW	$R$	Ref.	Comment
GRB 971214	yes	$22.06 \pm 0.06$	(1)	
GRB 000926	yes	$18.33 \pm 0.10$	(2)	Extrapolated from $R = 19.33$ at 20.7 hr using $\alpha = 1.69$
GRB 011211	yes	$20.23 \pm 0.04$	(3)	
GRB 021004	yes	$18.60 \pm 0.03$	(4)	
GRB 030323	yes	$19.00 \pm 0.1$	(5)	
GRB 050315	yes	$20.90 \pm 0.20$	(6)	
GRB 050401	UL	$23.00 \pm 0.10$	(7)	
GRB 050730	...	$20.20 \pm 0.1$	(8)	
GRB 050820A	UL	$18.78 \pm 0.14$	(6)	
GRB 050908	...	$22.38 \pm 0.10$	(9)	Data at 0.68, 4.25 and 22.12 hr, $\alpha = 0.78$
GRB 050922C	...	$19.98 \pm 0.03$	(6)	
GRB 060115	...	$21.77 \pm 0.12$	(10)	
GRB 060526	UL	$19.82 \pm 0.05$	(11)	
GRB 060604	UL	$21.40 \pm 0.30$	(12)	
GRB 060605	yes	$20.45 \pm 0.1$	(13)	
GRB 060607A	...	...	...	Unusual light curve — unable to interpolate
GRB 060707	yes	$21.30 \pm 0.30$	(14)	Interpolation between two datapoints
GRB 060714	UL	$21.10 \pm 0.1$	(15)	
GRB 060908	yes	$21.90 \pm 0.1$	(16)	
GRB 061110B	UL	$> 23.30$	(17)	Limit assuming $\alpha = 0.5$ from the VLT observation at 2.3 hr
GRB 070110	yes	$20.00 \pm 0.1$	(18)	Converted from $V$ -band
GRB 070506	yes	$> 20.14$	(19)	Limit assuming $\alpha = 0.5$ from the VLT observation at 3.6 hr
GRB 070611	...	$21.50 \pm 0.30$	(17)	Extrapolated from $R = 21.0$ at 7.7 hr adopting $\alpha = 1.0 \pm 0.5$
GRB 070721B	yes	$22.50 \pm 0.30$	(20)	Extrapolated from $R = 23.0 \pm 0.1$ at 17.6 hr adopting $\alpha = 1.0 \pm 0.5$
GRB 070802	UL	$23.50 \pm 0.1$	(21)	

NOTE.—The first 5 bursts are from the pre-*Swift* sample (Fynbo et al. 2003, and references therein), and the remaining 20 bursts are from the *Swift*-based sample studied in this work. The EW column indicates what type of information is available about the  $\text{Ly}\alpha$  EW of the host (detection, upper limit or no constraint); the actual values are given in Tables 3 and 5.  $R$  is the afterglow  $R$ -band magnitude at 12 hr after the burst. In the cases where we directly read the afterglow magnitude at 12 hr after the burst from a plot in the stated reference we have assigned a magnitude error of 0.1. The parameter  $\alpha$  is the slope of the light curve:  $F(t) \propto t^{-\alpha}$ .

References. — (1) Diercks et al. (1998); (2) Fynbo et al. (2001); (3) Jakobsson et al. (2004b); (4) Holland et al. (2003); (5) Vreeswijk et al. (2004); (6) Kann et al. (2010); (7) Watson et al. (2006); (8) Pandey et al. (2006); (9) Our measurement using archival data from ESO program 275.D-5022 (PI: Chincarini); (10) Our measurement using archival data from ESO program 076.A-0392 (PI: Tagliaferri); (11) Thöne et al. (2010); (12) Tanvir et al. (2006); (13) Ferrero et al. (2009); (14) de Ugarte Postigo et al. (2006) and Jakobsson et al. (2006a); (15) Krimm et al. (2007); (16) Covino et al. (2010); (17) Fynbo et al. (2009); (18) Troja et al. (2007); (19) Fynbo et al. (2009) but corrected for typo: correct value is  $R = 19.5$  at 3.6 hr; (20) Our measurement using data from our own ESO program 079.D-0429 (PI: Vreeswijk); (21) Krühler et al. (2008).

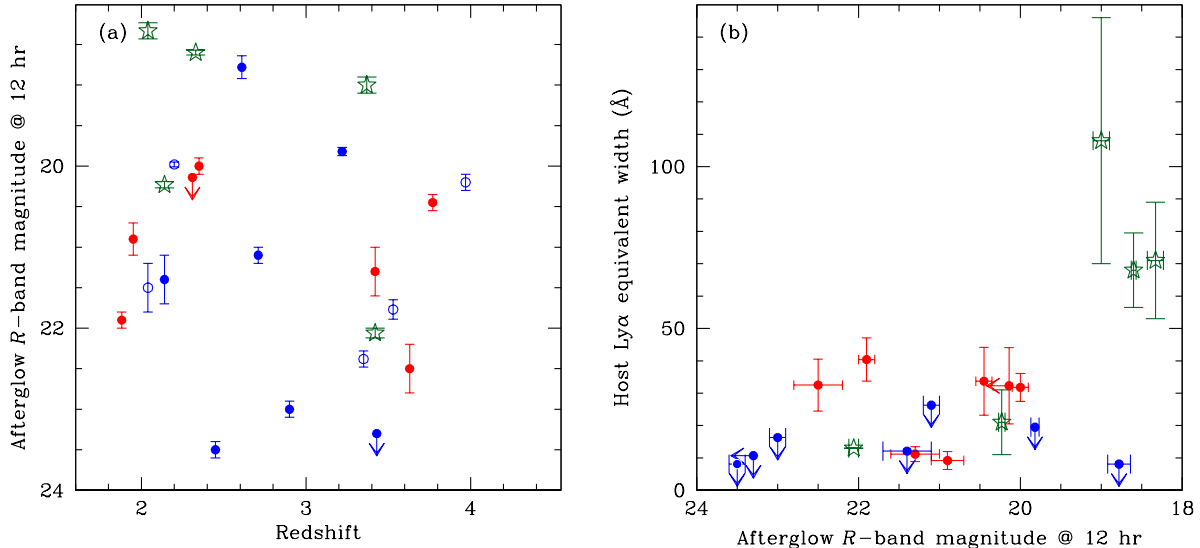


Fig. 10.— Afterglow  $R$ -band magnitude at 12 hr after the burst, versus redshift (panel a) and  $\text{Ly}\alpha$  EW (panel b). Open green stars: the pre-*Swift* sample of 5 GRB host  $\text{Ly}\alpha$  emitters. Other symbols: the sample of 20 hosts from this work: red filled circles: hosts with a  $\text{Ly}\alpha$  detection, blue filled circles: hosts without a  $\text{Ly}\alpha$  detection but with an upper limit on the  $\text{Ly}\alpha$  EW, blue open circles (panel a only): hosts with no constraints on the  $\text{Ly}\alpha$  EW.

$z \leq 4.5$  as considered here), where the optical is not cut off by inter-galactic medium absorption,  $\beta_{\text{OX}}$  is thus connected to dust extinction along the GRB sightline (e.g. Fynbo et al. 2009). In particular, assuming standard synchrotron theory,  $\beta_{\text{OX}}$  cannot be intrinsically smaller than 0.5, and therefore bursts with  $\beta_{\text{OX}} < 0.5$  are referred to as “dark bursts” (Jakobsson et al. 2004a), although moderate extinction can be present also in bursts with larger values of  $\beta_{\text{OX}}$ .

We have compiled a list of all known GRB hosts with  $\text{Ly}\alpha$  emission, both from this work and from the literature, including both pre-*Swift* and *Swift* bursts, see Table 5. The table lists both the afterglow  $\beta_{\text{OX}}$  and the host  $\text{Ly}\alpha$  emission properties. We have corrected the literature  $\text{Ly}\alpha$  fluxes for Galactic extinction where needed. The table only contains hosts with a  $\text{Ly}\alpha$  detection. The  $\text{Ly}\alpha$  upper limits from this work are in Table 3 (with  $\beta_{\text{OX}}$  available for all bursts from Fynbo et al. 2009).

In Fig. 11 we plot host  $\text{EW}(\text{Ly}\alpha)$  and host  $L(\text{Ly}\alpha)$  versus afterglow  $\beta_{\text{OX}}$ , both for the hosts from this work and for the additional hosts with  $\text{Ly}\alpha$  detections from the literature. The plots show a lack of hosts with high  $\text{EW}(\text{Ly}\alpha)$  and large

$L(\text{Ly}\alpha)$  at the low end of the  $\beta_{\text{OX}}$  range. This indicates that dust extinction is important in reducing the strength of the  $\text{Ly}\alpha$  line. GRB 061222A goes against the trend, with a very low  $\beta_{\text{OX}}$  (namely an upper limit<sup>13</sup> of  $\beta_{\text{OX}} < 0.22$ ) and detected  $\text{Ly}\alpha$  emission. This can be explained by the fact that  $\beta_{\text{OX}}$  only probes the afterglow sightline, whereas the host  $\text{Ly}\alpha$  emission is a quantity that is global for the galaxy. There are indeed several cases where a dark GRB exploded in an overall blue galaxy, e.g. GRB 070306 (Jaunsen et al. 2008) and GRB 100621A (Krühler et al. 2011). It is also seen from Fig. 11 that the hosts of the pre-*Swift* GRBs with high  $\text{EW}(\text{Ly}\alpha)$  and large  $L(\text{Ly}\alpha)$  are preferentially found at the high end of the  $\beta_{\text{OX}}$  range. This suggests that the pre-*Swift* sample (shown as open green stars in Fig. 11) discussed by Fynbo et al. (2003) is more biased against dusty sightlines.

Our finding that  $\text{Ly}\alpha$  emission is not ubiq-

<sup>13</sup>The upper limit comes from the afterglow only having an  $R$ -band upper limit. The afterglow has a  $K_s$ -band detection (Cenko & Fox 2006), which gives  $\beta_{\text{OX}} = 0.10$  (with “O” now signifying  $K_s$ -band rather than optical/ $R$ -band), which is even more constraining.

TABLE 5  
 KNOWN GRB HOST  $\text{Ly}\alpha$  EMITTERS: AFTERGLOW SPECTRAL SLOPE AND HOST  $\text{Ly}\alpha$  PROPERTIES

Name	$z$	T	$\beta_{\text{OX}}$	Ref.	EW( $\text{Ly}\alpha$ )	Ref.	$F(\text{Ly}\alpha)$	Ref.	$L(\text{Ly}\alpha)$	$v(\text{Ly}\alpha)$	Ref.
GRB 971214	3.42	no	0.64	(1)	13	(6)	$6.2 \pm 0.7$	(13)	$0.66 \pm 0.07$	...	...
GRB 000926	2.04	no	0.87	(1)	$71 \pm 18$	(7)	$149 \pm 11^{\text{b}}$	(7)	$4.51 \pm 0.33$	...	...
GRB 011211	2.14	no	0.98	(1)	$21 \pm 10$	(8)	$33.6 \pm 9.6^{\text{b}}$	(8)	$1.14 \pm 0.33$	...	...
GRB 021004	2.33	no	0.93	(1)	$68 \pm 11.5$	(9)	$313 \pm 64^{\text{b}}$	(14)	$13.14 \pm 2.67$	530	(14)
GRB 030323	3.37	no	...	...	$108 \pm 38$	(10)	$12 \pm 1$	(15)	$1.23 \pm 0.10$	$151 \pm 46$	(15)
GRB 050315	1.95	yes	0.63	(2)	$9.2 \pm 2.8$	(11)	$23.4 \pm 6.8$	(11)	$0.64 \pm 0.19$	$283 \pm 62$	(11)
GRB 060605	3.77	yes	1.00	(2)	$33.7 \pm 10.5$	(11)	$17.0 \pm 2.7$	(11)	$2.28 \pm 0.36$	$620 \pm 26$	(11)
GRB 060707	3.42	yes	0.73	(2)	$11.2 \pm 2.3$	(11)	$16.5 \pm 3.1$	(11)	$1.75 \pm 0.33$	$742 \pm 38$	(11)
GRB 060714	2.71	yes	0.77	(2)	...	...	$17.3^{\text{b}}$	(16)	1.05	...	...
GRB 060908	1.88	yes	0.80	(3)	$40.4 \pm 6.7$	(11)	$77.8 \pm 9.5$	(11)	$1.94 \pm 0.24$	$347 \pm 31$	(11)
GRB 060926	3.21	no	0.87	(4)	...	...	$62.1 \pm 4.9^{\text{b}}$	(17)	$5.65 \pm 0.45$	311	(17)
GRB 061222A	2.09	no	$<0.22$	(2)	31	(12)	$168^{\text{b}}$	(18)	5.39	...	...
GRB 070110	2.35	yes	0.77	(2)	$31.8 \pm 4.3$	(11)	$40.2 \pm 4.0$	(11)	$1.73 \pm 0.17$	$358 \pm 26$	(11)
GRB 070506	2.31	yes	0.93	(2)	$32.3 \pm 11.8$	(11)	$13.9 \pm 3.5$	(11)	$0.57 \pm 0.14$	$360 \pm 62$	(11)
GRB 070721B	3.63	yes	0.72	(2)	$32.5 \pm 8.0^{\text{a}}$	(11)	$11.2 \pm 1.6$	(11)	$1.37 \pm 0.19$	$212 \pm 31$	(11)
GRB 071031	2.69	no	0.97	(2)	...	...	$23.6 \pm 2.7^{\text{b}}$	(17)	$1.41 \pm 0.16$	254	(17)
GRB 090205	4.65	no	0.98	(5)	...	...	$23.6 \pm 4.9^{\text{b}}$	(19)	$5.17 \pm 1.08$	$180 \pm 153$	(19)

<sup>a</sup>The listed error reflects the random error only. A systematic error due to the fitting and subtraction of a neighboring object is likely present.

<sup>b</sup>The published  $\text{Ly}\alpha$  flux or the provided spectrum was not corrected for Galactic extinction, but we have applied the correction.

NOTE.—T indicates whether the host is part of the TOUGH sample (§2.1; Hjorth et al. 2012) studied in this work.  $\beta_{\text{OX}}$  is the afterglow optical-to-X-ray spectral slope (see Eq. 6), where optical means  $R$ -band (unless otherwise stated) and X-ray means 3 keV. EW( $\text{Ly}\alpha$ ) is the rest-frame  $\text{Ly}\alpha$  emission line EW, in Å.  $F(\text{Ly}\alpha)$  is the  $\text{Ly}\alpha$  emission line flux, in units of  $10^{-18} \text{ erg cm}^{-2} \text{ s}^{-1}$ .  $L(\text{Ly}\alpha)$  is the  $\text{Ly}\alpha$  emission line luminosity, in units of  $10^{42} \text{ erg s}^{-1}$ .  $v(\text{Ly}\alpha)$  is the rest-frame velocity centroid of the  $\text{Ly}\alpha$  emission line with respect to the afterglow redshift, in  $\text{km s}^{-1}$ . “Ref.” gives the reference for the preceding column. The bursts up to and including GRB 030323 are pre-*Swift*, while the remaining bursts are from *Swift*. All  $\text{Ly}\alpha$  fluxes and luminosities are corrected for Galactic extinction. Note that GRB 030429 is not included, since even though its spectrum showed an indication of  $\text{Ly}\alpha$  emission, it was not statistically significant ( $\lesssim 2\sigma$ ) (Jakobsson et al. 2004c).

References. — (1) Jakobsson et al. (2004a); (2) Fynbo et al. (2009); (3) Our calculation, using  $R$ -band data from Covino et al. (2010) and X-ray data from Evans et al. (2007, 2009) (we note that the  $\beta_{\text{OX}}$  value in Fynbo et al. 2009 is in error); (4) Our calculation, using archival  $R$ -band data from ESO program 077.D-0805 (PI: Tagliaferri) and X-ray data from Evans et al. (2007, 2009); (5) Our calculation, using  $I$ -band photometry from D’Avanzo et al. (2010) (rather than  $R$ -band, due to the high redshift) and X-ray data from Evans et al. (2007, 2009); (6) Our measurement, using the host spectrum from Kulkarni et al. (1998); (7) Fynbo et al. (2002), with  $F(\text{Ly}\alpha)$  corrected for continuum contribution as prescribed in that paper; (8) Fynbo et al. (2003); (9) Jakobsson et al. (2005); (10) Our calculation, using the line flux from Vreeswijk et al. (2004) and deriving the continuum flux density from the F606W photometry from Wainwright et al. (2007) (correcting for  $\text{Ly}\alpha$  forest absorption and imposing a slitloss; these effects almost cancel out); (11) This work; (12) Our measurement, using the host spectrum from Perley et al. (2009); (13) Kulkarni et al. (1998); (14) Møller et al. (2002); (15) Vreeswijk et al. (2004); (16) Jakobsson et al. (2006b); (17) Our measurement, using the afterglow spectrum from Fynbo et al. (2009); (18) D. Perley, priv. comm., cf. Perley et al. (2009); (19) D’Avanzo et al. (2010).

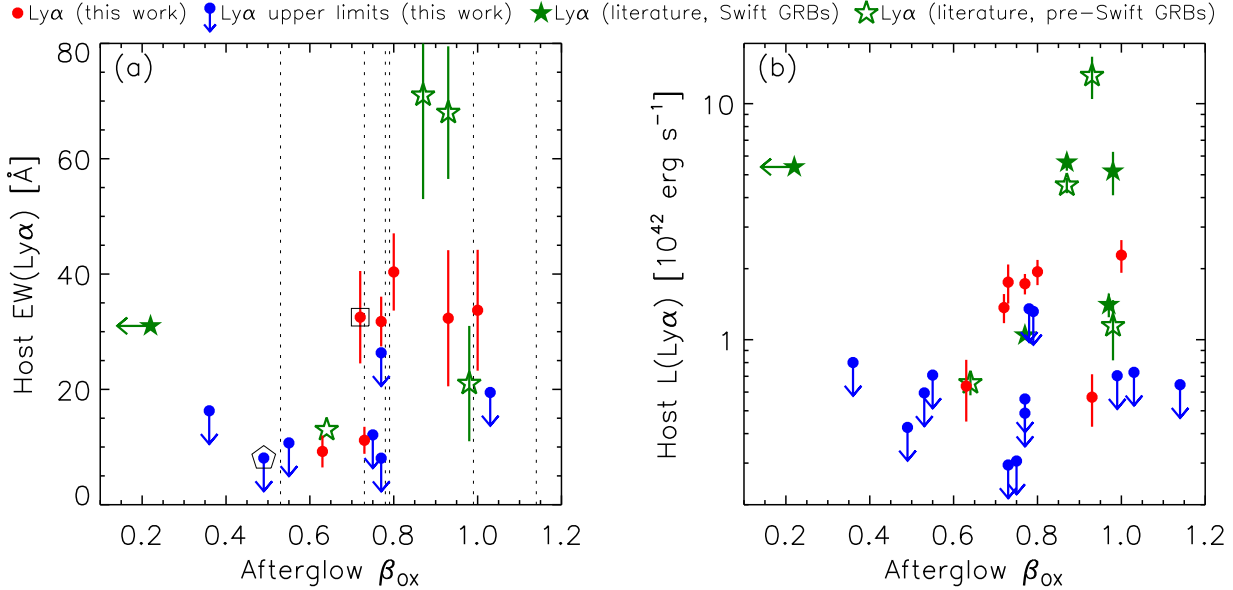


Fig. 11.— Host Ly $\alpha$  EW (panel a) and host Ly $\alpha$  luminosity (panel b) versus afterglow spectral index  $\beta_{\text{OX}}$ . The GRBs in the sample of this paper are shown as red filled circles (Ly $\alpha$  detections), blue upper limits (Ly $\alpha$  non-detections), and dotted lines (unconstrained Ly $\alpha$  EWs, panel a only). Additional GRB hosts with Ly $\alpha$  detections from the literature are shown as green stars (open stars: pre-*Swift*, filled stars: *Swift*). These bursts are not in the sample of this paper, except for GRB060714: this burst has a Ly $\alpha$  detection from the literature, whereas our data resulted in an upper limit, as discussed in §3.3. This burst is therefore plotted twice (panel b only): as a detection and as an upper limit. Some of the literature bursts plotted in panel (b) are absent from panel (a) due to not having a measured EW, which in turn is due to only an afterglow spectrum being available. The plotted data for all the Ly $\alpha$  detections (both from this work and from the literature) are given in Table 5. The non-detections (this work only) are given in Table 3, with  $\beta_{\text{OX}}$  taken from Fynbo et al. (2009). Note that GRB 030323 (listed in Table 5) is not plotted here due to not having X-ray observations and hence no  $\beta_{\text{OX}}$ . The two systems where a neighboring object was fitted and subtracted are marked: GRB 070721B (box) and GRB 070802 (pentagon). Note the logarithmic axis for the Ly $\alpha$  luminosity.

uitous among GRB host galaxies has implications on how well GRBs trace the overall massive star-formation activity and on the nature of GRB progenitors. Given that Ly $\alpha$  photons are more easily destroyed by dust than other UV photons due to resonant scattering, it has been argued that GRB hosts have low dust content. This could be due, among other reasons, to low metallicity, in agreement with the prediction of the collapsar model (MacFadyen & Woosley 1999; Yoon & Langer 2005; Woosley & Heger 2006). Our analysis of a larger sample of GRB hosts shows that Ly $\alpha$  emission is less ubiquitous than previously found based on a much smaller sample (Fynbo et al. 2003; Jakobsson et al. 2005), so that the above argument is not valid. Whereas other mechanisms than dust can reduce the strength of the Ly $\alpha$  line (e.g. the geometry of the interstellar medium), the trend visible in Fig. 11 suggests that the strength of the Ly $\alpha$  line is related to the presence of dust. We note that the objects in the sample studied in this work all have a redshift measured from the optical afterglow, hence they are biased against very dusty systems. If the connection between the presence of dust and the weakness of the Ly $\alpha$  line holds, we expect that the hosts of optically-obscured (i.e. dark) GRBs should have even less prominent Ly $\alpha$  emission.

The recent work of Krühler et al. (2012) provides additional insight. VLT/X-shooter was used to target several TOUGH hosts that lacked redshifts. For 7 of the TOUGH hosts the found redshift was in the range  $z = 1.8$ – $4.5$ , and these are thus hosts missed by the target selection for this work (cf. §2.2). The redshifts were based on detecting one or more of the following emission lines: [O II], H $\beta$ , [O III] and H $\alpha$ . In no cases was Ly $\alpha$  detected. These 7 bursts mostly have low  $\beta_{\text{OX}}$  values<sup>14</sup>. While the lack of Ly $\alpha$  emission still has to be quantified in terms of upper limits on the EWs, the Krühler et al. (2012) result supports the picture that weak or absent Ly $\alpha$  emission is at least in part caused by dust.

The Dark Cosmology Centre is funded by the

<sup>14</sup>The  $\beta_{\text{OX}}$  values are: GRB 050819:  $<0.90$ , GRB 050915A:  $<0.44$ , GRB 051001:  $<0.56$ , GRB 060814:  $<-0.06$ , GRB 070103:  $<0.48$ , GRB 070129:  $0.62$ , and GRB 070419B:  $0.25$  (Fynbo et al. 2009, and references therein).

Danish National Research Foundation. BMJ and JPUF acknowledge support from the ERC-StG grant EGG-278202. This research has made use of the NASA/IPAC Extragalactic Database (NED) which is operated by the Jet Propulsion Laboratory, California Institute of Technology, under contract with the National Aeronautics and Space Administration. This work made use of data supplied by the UK Swift Science Data Centre at the University of Leicester. We thank S. George Djorgovski for providing the spectrum of the GRB 971214 host and Dan Perley for providing the spectrum of the GRB 061222A host, cf. Table 5. Peter Laursen is thanked for discussions about Ly $\alpha$  radiative transfer. Alice E. Shapley is thanked for discussions and for providing the data on the LBGs from Shapley et al. (2003) in machine-readable format. Thomas Krühler is thanked for discussions about the X-shooter host spectroscopy. We thank the anonymous referee for comments that helped improve the presentation.

*Facilities:* VLT (FORs1).

## REFERENCES

- Adams, T. F. 1972, ApJ, 174, 439
- Adelberger, K. L., Steidel, C. C., Shapley, A. E., & Pettini, M. 2003, ApJ, 584, 45
- Appenzeller, I., Fricke, K., Furtig, W., et al. 1998, The Messenger, 94, 1
- Berger, E., & Becker, G. 2005, GRB Coordinates Network, 3520, 1
- Berger, E., Kulkarni, S. R., Fox, D. B., et al. 2005, ApJ, 634, 501
- Blanton, M. R., & Roweis, S. 2007, AJ, 133, 734
- Brocklehurst, M. 1971, MNRAS, 153, 471
- Cardelli, J. A., Clayton, G. C., & Mathis, J. S. 1989, ApJ, 345, 245
- Cassata, P., Le Fèvre, O., Garilli, B., et al. 2011, A&A, 525, A143+
- Castro-Tirado, A. J., Amado, P., Negueruela, I., et al. 2006, GRB Coordinates Network, 5218, 1
- Cenko, S. B., & Fox, D. B. 2006, GRB Coordinates Network, 5978, 1

- Charlot, S., & Fall, S. M. 1993, *ApJ*, 415, 580
- Chary, R., Berger, E., & Cowie, L. 2007, *ApJ*, 671, 272
- Chen, H.-W., Prochaska, J. X., Bloom, J. S., & Thompson, I. B. 2005, *ApJ*, 634, L25
- Covino, S., Campana, S., Conciatore, M. L., et al. 2010, *A&A*, 521, A53+
- D’Avanzo, P., Perri, M., Fugazza, D., et al. 2010, *A&A*, 522, A20+
- de Ugarte Postigo, A., Gorosabel, J., Jelinek, M., et al. 2006, *GRB Coordinates Network*, 5290, 1
- Diercks, A. H., Deutsch, E. W., Castander, F. J., et al. 1998, *ApJ*, 503, L105+
- Douglas, L. S., Bremer, M. N., Lehnert, M. D., Stanway, E. R., & Milvang-Jensen, B. 2010, *MNRAS*, 409, 1155
- Elíasdóttir, Á., Fynbo, J. P. U., Hjorth, J., et al. 2009, *ApJ*, 697, 1725
- Evans, P. A. 2011, *GRB Coordinates Network*, 12250, 1
- Evans, P. A., & Osborne, J. P. 2011, *GRB Coordinates Network*, 12273, 1
- Evans, P. A., Beardmore, A. P., Page, K. L., et al. 2007, *A&A*, 469, 379
- . 2009, *MNRAS*, 397, 1177
- Ferrero, P., Klose, S., Kann, D. A., et al. 2009, *A&A*, 497, 729
- Finkelstein, S. L., Papovich, C., Salmon, B., et al. 2011, *ApJ*, submitted, arXiv:1110.3785
- Fox, A. J., Ledoux, C., Vreeswijk, P. M., Smette, A., & Jaunsen, A. O. 2008, *A&A*, 491, 189
- Fukugita, M., Shimasaku, K., & Ichikawa, T. 1995, *PASP*, 107, 945
- Fynbo, J. P. U., Møller, P., Thomsen, B., et al. 2002, *A&A*, 388, 425
- Fynbo, J. P. U., Jakobsson, P., Møller, P., et al. 2003, *A&A*, 406, L63
- Fynbo, J. P. U., Jakobsson, P., Prochaska, J. X., et al. 2009, *ApJS*, 185, 526
- Fynbo, J. P. U., Laursen, P., Ledoux, C., et al. 2010, *MNRAS*, 408, 2128
- Fynbo, J. U., Gorosabel, J., Dall, T. H., et al. 2001, *A&A*, 373, 796
- Giavalisco, M., Koratkar, A., & Calzetti, D. 1996, *ApJ*, 466, 831
- Gronwall, C., Ciardullo, R., Hickey, T., et al. 2007, *ApJ*, 667, 79
- Grove, L. F., Fynbo, J. P. U., Ledoux, C., et al. 2009, *A&A*, 497, 689
- Hamuy, M., Suntzeff, N. B., Heathcote, S. R., et al. 1994, *PASP*, 106, 566
- Hamuy, M., Walker, A. R., Suntzeff, N. B., et al. 1992, *PASP*, 104, 533
- Hansen, M., & Oh, S. P. 2006, *MNRAS*, 367, 979
- Harrington, J. P. 1973, *MNRAS*, 162, 43
- Hayes, M., Östlin, G., Mas-Hesse, J. M., et al. 2005, *A&A*, 438, 71
- Hjorth, J., & Bloom, J. S. 2012, in *Gamma-ray Bursts*, eds. Kouveliotou, Wijers & Woosley, Cambridge University Press, in press, arXiv:1104.2274
- Hjorth, J., Sollerman, J., Møller, P., et al. 2003, *Nature*, 423, 847
- Hjorth, J., Malesani, D., Jakobsson, P., et al. 2012, *ApJ*, submitted, arXiv:1205.3162
- Holland, S. T., Weidinger, M., Fynbo, J. P. U., et al. 2003, *AJ*, 125, 2291
- Jakobsson, P., Hjorth, J., Fynbo, J. P. U., et al. 2004a, *ApJ*, 617, L21
- Jakobsson, P., Malesani, D., Hjorth, J., Fynbo, J. P. U., & Milvang-Jensen, B. 2011, *Astronomische Nachrichten*, 332, 276
- Jakobsson, P., Tanvir, N., Jensen, B. L., et al. 2006a, *GRB Coordinates Network*, 5298, 1
- Jakobsson, P., Hjorth, J., Ramirez-Ruiz, E., et al. 2004b, *New A*, 9, 435
- Jakobsson, P., Hjorth, J., Fynbo, J. P. U., et al. 2004c, *A&A*, 427, 785



- Jakobsson, P., Björnsson, G., Fynbo, J. P. U., et al. 2005, *MNRAS*, 362, 245
- Jakobsson, P., Fynbo, J. P. U., Ledoux, C., et al. 2006b, *A&A*, 460, L13
- Jakobsson, P., Hjorth, J., Malesani, D., et al. 2012, *ApJ*, in press, arXiv:1205.3490
- Jaunsen, A. O., Rol, E., Watson, D. J., et al. 2008, *ApJ*, 681, 453
- Kann, D. A., Klose, S., Zhang, B., et al. 2010, *ApJ*, 720, 1513
- Kennicutt, R. C. 1998, *ARA&A*, 36, 189
- Krimm, H. A., Granot, J., Marshall, F. E., et al. 2007, *ApJ*, 665, 554
- Krühler, T., Küpcü Yoldaş, A., Greiner, J., et al. 2008, *ApJ*, 685, 376
- Krühler, T., Greiner, J., Schady, P., et al. 2011, *A&A*, 534, A108
- Krühler, T., Malesani, D., Milvang-Jensen, B., et al. 2012, *ApJ*, submitted, arXiv:1205.4036
- Kulkarni, S. R., Djorgovski, S. G., Ramaprakash, A. N., et al. 1998, *Nature*, 393, 35
- Landolt, A. U. 1992, *AJ*, 104, 340
- Laursen, P., Sommer-Larsen, J., & Andersen, A. C. 2009, *ApJ*, 704, 1640
- MacFadyen, A. I., & Woosley, S. E. 1999, *ApJ*, 524, 262
- Malesani, D., et al. 2012, *ApJ*, in prep.
- Markwardt, C. B. 2009, in *Astronomical Society of the Pacific Conference Series*, Vol. 411, *Astronomical Society of the Pacific Conference Series*, ed. D. A. Bohlender, D. Durand, & P. Dowler, 251–254
- McLinden, E. M., Finkelstein, S. L., Rhoads, J. E., et al. 2011, *ApJ*, 730, 136
- Michalowski, M. J., Kamble, A., Hjorth, J., et al. 2012, *ApJ*, submitted, arXiv:1205.4239
- Milvang-Jensen, B., Noll, S., Halliday, C., et al. 2008, *A&A*, 482, 419
- Møller, P., Fynbo, J. P. U., Hjorth, J., et al. 2002, *A&A*, 396, L21
- Moré, J. J. 1978, in *Lecture Notes in Mathematics*, Vol. 630, *Numerical Analysis, Proceedings of the Biennial Conference Held at Dundee, June 28–July 1, 1977*, ed. G. A. Watson, 105–116
- Neufeld, D. A. 1991, *ApJ*, 370, L85
- Niino, Y., Totani, T., & Kobayashi, M. A. R. 2009, *ApJ*, 707, 1634
- Nilsson, K. K., Tapken, C., Møller, P., et al. 2009, *A&A*, 498, 13
- O’Donnell, J. E. 1994, *ApJ*, 422, 158
- Oke, J. B. 1990, *AJ*, 99, 1621
- Pandey, S. B., Castro-Tirado, A. J., McBreen, S., et al. 2006, *A&A*, 460, 415
- Patat, F. 2003, *A&A*, 400, 1183
- Perley, D. A., Cenko, S. B., Bloom, J. S., et al. 2009, *AJ*, 138, 1690
- Pettini, M., Steidel, C. C., Adelberger, K. L., Dickinson, M., & Giavalisco, M. 2000, *ApJ*, 528, 96
- Piranomonte, S., Ward, P. A., Fiore, F., et al. 2008, *A&A*, 492, 775
- Press, W. H., Teukolsky, S. A., Vetterling, W. T., & Flannery, B. P. 1992, *Numerical recipes in FORTRAN. The art of scientific computing* (Cambridge: Cambridge University Press, 2nd ed.)
- Prochaska, J. X., Chen, H.-W., Bloom, J. S., et al. 2007, *ApJS*, 168, 231
- Rauch, M., Haehnelt, M., Bunker, A., et al. 2008, *ApJ*, 681, 856
- Rol, E., Jakobsson, P., Tanvir, N., & Levan, A. 2006, *GRB Coordinates Network*, 5555, 1
- Salvaterra, R., Della Valle, M., Campana, S., et al. 2009, *Nature*, 461, 1258
- Schlegel, D. J., Finkbeiner, D. P., & Davis, M. 1998, *ApJ*, 500, 525

- Schwarz, H. E., & Melnick, J. 1993, in *The ESO Users' Manual*, 19–24
- Shapley, A. E., Steidel, C. C., Pettini, M., & Adelberger, K. L. 2003, *ApJ*, 588, 65
- Stanek, K. Z., Matheson, T., Garnavich, P. M., et al. 2003, *ApJ*, 591, L17
- Stark, D. P., Ellis, R. S., & Ouchi, M. 2011, *ApJ*, 728, L2+
- Steidel, C. C., & Hamilton, D. 1993, *AJ*, 105, 2017
- Tanvir, N., Rol, E., & Hewett, P. 2006, *GRB Coordinates Network*, 5216, 1
- Tanvir, N. R., Fox, D. B., Levan, A. J., et al. 2009, *Nature*, 461, 1254
- Thöne, C. C., Perley, D. A., Cooke, J., et al. 2007, *GRB Coordinates Network*, 6741, 1
- Thöne, C. C., Kann, D. A., Jóhannesson, G., et al. 2010, *A&A*, 523, A70+
- Troja, E., Cusumano, G., O'Brien, P. T., et al. 2007, *ApJ*, 665, 599
- Tüg, H. 1977, *The Messenger*, 11, 7
- Valls-Gabaud, D. 1993, *ApJ*, 419, 7
- van Dokkum, P. G. 2001, *PASP*, 113, 1420
- Verhamme, A., Schaerer, D., & Maselli, A. 2006, *A&A*, 460, 397
- Vreeswijk, P. M., Ellison, S. L., Ledoux, C., et al. 2004, *A&A*, 419, 927
- Wainwright, C., Berger, E., & Penprase, B. E. 2007, *ApJ*, 657, 367
- Watson, D., Fynbo, J. P. U., Ledoux, C., et al. 2006, *ApJ*, 652, 1011
- Wijers, R. A. M. J., Bloom, J. S., Bagla, J. S., & Natarajan, P. 1998, *MNRAS*, 294, L13
- Wosley, S. E., & Bloom, J. S. 2006, *ARA&A*, 44, 507
- Wosley, S. E., & Heger, A. 2006, *ApJ*, 637, 914
- Yoon, S., & Langer, N. 2005, *A&A*, 443, 643

### A. Observations obtained of systems not in the TOUGH sample

Three systems which were not in the final TOUGH sample were also observed, see Table 6. The reason for these 3 systems not being in the TOUGH sample are as follows: GRB 050603 and GRB 060223A did not have an XRT position distributed within 12 hours (although an XRT observation had been made within 12 hours), and GRB 070810A did not have a Sun distance greater than  $55^\circ$  (its Sun distance was  $49^\circ$ ). The TOUGH sample criteria are described in Hjorth et al. (2012) and are summarised in §2.1.

The spectra are shown in Fig. 12 (2D spectra), Fig. 13 (1D spectra) and Fig. 14 (spatial profiles). For none of these systems neither the continuum nor the Ly $\alpha$  emission line were detected, see Table 7.

For GRB 050603 the afterglow redshift of  $z = 2.821$  from Berger & Becker (2005) is likely wrong: it was derived based on a reported bright emission line interpreted as Ly $\alpha$  in the afterglow spectrum (0.75 hr exposure with Magellan/IMACS), but in our deep host spectrum (2.2 hr exposure with VLT/FORS1) we do not detect any emission; we derive a  $3\sigma$  upper limit on the Ly $\alpha$  flux at  $z = 2.821$  of  $4.7 \times 10^{-18} \text{ erg s}^{-1} \text{ cm}^{-2}$  (cf. Table 7). We do not find an emission line at any other redshift.

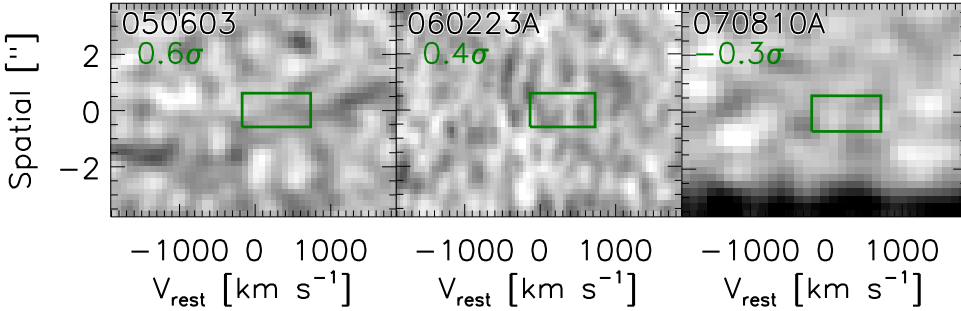


Fig. 12.— 2D spectra for the 3 systems not in the TOUGH sample. See Fig. 4 for further information.

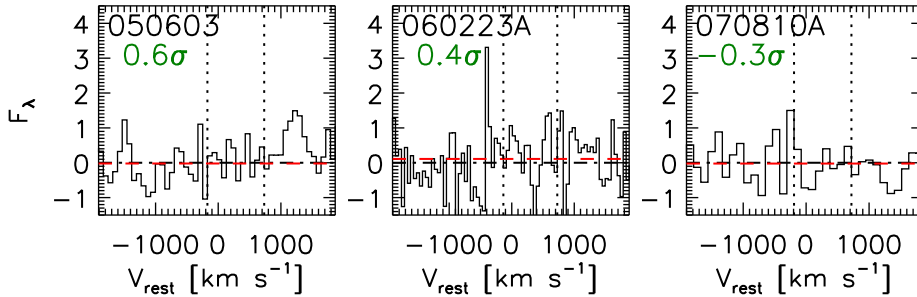


Fig. 13.— 1D spectra for the 3 systems not in the TOUGH sample. See Fig. 5 for further information.

TABLE 6  
OBSERVED SYSTEMS NOT IN THE TOUGH SAMPLE

Name	$z$	Ref.	$R_{\text{host}}$ (mag)	Grism+filter	CCD	$T_{\text{exp}}^{\text{total}}$ (hr)	Seeing (arcsec)	$A_V$ (mag)
GRB 050603	N/A <sup>a</sup>	(1)	> 26.6	600B	old	2.2	< 1.1	0.092
GRB 060223A	4.406	(2)	> 26.3	600R+GG435	old	2.1	0.7	0.389
GRB 070810A	2.17	(3)	> 26.7	600B	new	1.5	0.7	0.072

<sup>a</sup>The redshift  $z = 2.821$  for GRB 050603 from Berger & Becker (2005) is likely wrong: it was derived based on a reported very bright emission line interpreted as Ly $\alpha$  in the afterglow spectrum, but in our deep host spectrum we do not detect any Ly $\alpha$  emission; we derive a  $3\sigma$  upper limit on the Ly $\alpha$  flux at  $z = 2.821$  of  $4.7 \times 10^{-18} \text{ erg s}^{-1} \text{ cm}^{-2}$  (cf. Table 7).

NOTE.—See Table 1 for further information.

References. — (1) Berger & Becker (2005); (2) Chary et al. (2007); (3) Thöne et al. (2007).

TABLE 7  
LY $\alpha$  MEASUREMENTS FROM THE SPECTRA

Name	Ly $\alpha$ aperture				$F(\text{Ly}\alpha)$	$L(\text{Ly}\alpha)$	$F_\lambda(\text{cont.})$	EW(Ly $\alpha$ )	$v(\text{Ly}\alpha)$
	$c(v)$	$c(s)$	$w(v)$	$w(s)$					
(1)	(2)	(3)	(4)	(5)	(6)	(7)	(8)	(9)	(10)
GRB 050603	281	0.02	906	1.20	< 9.3	< 0.62	< 9.0	...	...
GRB 060223A	297	0.00	862	1.20	< 14.5	< 2.80	< 12.6	...	...
GRB 070810A	264	-0.05	912	1.25	< 8.7	< 0.31	< 9.5	...	...

NOTE.—See Table 3 for further information.

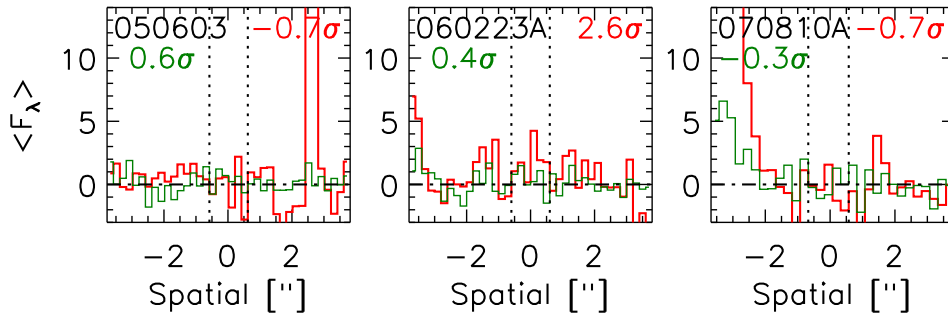


Fig. 14.— Spatial profiles of the 3 systems not in the TOUGH sample. See Fig. 6 for further information.